International Journal of Psychophysiology 97 (2015) 189–209

Contents lists available at ScienceDirect

International Journal of Psychophysiology

journal homepage: www.elsevier.com/locate/ijpsycho

Review

Issues and considerations for using the scalp surface Laplacian in EEG/ERP research: A tutorial review

Jürgen Kayser *, Craig E. Tenke

[a] Division of Cognitive Neuroscience, New York State Psychiatric Institute, New York, NY, USA
[b] Department of Psychiatry, Columbia University College of Physicians & Surgeons, New York, NY, USA

ARTICLE INFO

Article history:
Received 14 November 2014
Received in revised form 26 March 2015
Accepted 13 April 2015
Available online 25 April 2015

Keywords:
Current source density (CSD)
EEG recording reference
EEG spectra
Event-related potentials (ERPs)
ERP component
Surface Laplacian (SL)
Spherical spline interpolation
Volume conduction

ABSTRACT

Despite the recognition that the surface Laplacian may counteract adverse effects of volume conduction and recording reference for surface potential data, electrophysiology as a discipline has been reluctant to embrace this approach for data analysis. The reasons for such hesitation are manifold but often involve unfamiliarity with the nature of the underlying transformation, as well as intimidation by a perceived mathematical complexity, and concerns of signal loss, dense electrode array requirements, or susceptibility to noise. We revisit the pitfalls arising from volume conduction and the mandated arbitrary choice of EEG reference, describe the basic principle of the surface Laplacian transform in an intuitive fashion, and exemplify the differences between common reference schemes (nose, linked mastoids, average) and the surface Laplacian for frequently-measured EEG spectra (theta, alpha) and standard event-related potential (ERP) components, such as N1 or P3. We specifically review common reservations against the universal use of the surface Laplacian, which can be effectively addressed by employing spherical spline interpolations with an appropriate selection of the spline flexibility parameter and regularization constant. We argue from a pragmatic perspective that not only are these reservations unfounded but that the continued predominant use of surface potentials poses a considerable impediment on the progress of EEG and ERP research.

1. Introduction

Since its original discovery and the first published paper of Berger (1929), the electroencephalogram (EEG) has become an ubiquitous diagnostic utility and research tool of remarkable impact in clinical praxis (e.g., Shibasaki et al., 2014) and basic neuroscience (e.g., Gevins, 1998) alike. Among the diverse neuroimaging methods that have more recently become available, EEG is unique in its combined ability to represent neuronal activity 1) directly (i.e., without relying on an intermediate response system) and 2) in real time, while also being 3) non-invasive and 4) comparatively inexpensive. Because EEG is a time-varying voltage measure (i.e., potential difference) of electrical fields, it is limited by the fact that measuring potentials always require a point of reference (i.e., the EEG is reference-dependent) and by the circumstance that electrical fields originating from any neuronal structure will influence the electrical potential throughout the brain and surrounding physiological tissue (i.e., the EEG signal is a mixture of sources and is smeared by volume conduction). Both of these limitations can be mitigated by use of the surface Laplacian (SL), which is a simple mathematical transformation applied to the EEG surface potentials.

The main objective of this tutorial review is to introduce the use of SL to EEG researchers unfamiliar with or currently skeptical of this approach, and to argue for the routine use of SL methods in EEG research from a pragmatic perspective. For this purpose, we first visually illustrate the EEG reference problem and its impact on event-related potential (ERP) data analysis. Second, we show how the SL transformation works in principle, building on simple one-dimensional and two-dimensional (local Hjorth) Laplacian implementations to offer an intuitive description of SL computation via spherical splines, along with general considerations for practical use in EEG studies. Third, we provide a side-by-side comparison of typical EEG and ERP measures using reference-dependent surface potentials and their SL counterparts, including alpha and theta power, auditory P3(00), visual N1, mismatch negativity (MMN), and ERN-like activations (components). Finally, we revisit and directly address previous reservations regarding the use of the SL, including concerns that SL measures represent activations at a different spatial scale than surface potentials. However, it is beyond

Abbreviations: AR, average reference; CRN, correct response negativity; CSD, current source density; CV, cross-validation; EEG, electroencephalogram; ERN, error-related negativity; ERP, event-related potentials; FRN, mid-frontal response-related negativity; ICA, independent components analysis; λ, spline regularization constant (lambda); LM, linked-mastoids reference; *m*, spline flexibility constant (spline order); MMN, mismatch negativity; NR, nose reference; PCA, principal components analysis; REST, reference electrode standardization technique; SCD, scalp current density; SP, surface potential; SL, surface Laplacian.

* Corresponding author at: New York State Psychiatric Institute, Division of Cognitive Neuroscience, Unit 50, 1051 Riverside Drive, New York, NY 10032, USA. Tel.: +1 646 774 5207; fax: +1 212 543 6540.
E-mail address: kayserj@nyspi.columbia.edu (J. Kayser).

http://dx.doi.org/10.1016/j.ijpsycho.2015.04.012
0167-8760/

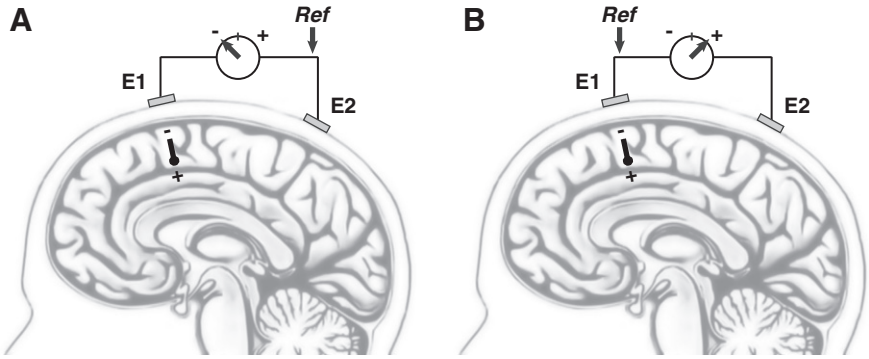

Fig. 1. Schematic sagittal view of the brain with two scalp electrodes (E1, E2). (A) Given a cortical dipole pointing with its negative pole towards E1, a negative potential is measured by the voltage meter for site E1 if site E2 serves as the recording reference (Ref). (B) For the same dipole, a positive potential is measured for E2 if E1is used as the reference. In either case, however, the measured potential difference indicates that E2 is more positive than E1.

the scope of this paper to detail the neurophysiological and neuroanatomical underpinnings of EEG phenomena recorded at scalp, which are covered in depth elsewhere (e.g., Nunez, 1981; Nunez and Srinivasan, 2006), or how patterns of neuronal activation are differentially represented by scalp or intracranial Laplacian estimates (Tenke and Kayser, 2012).

1.1. Implications of the EEG reference

The EEG signal reflects the summation of many ($>10^7$) synchronously activated cortical neurons that have similar spatial orientation, and their combined activity may be conveniently conceptualized (or simplified) as a current dipole with respect to the macroscopic scale of the scalp-recorded EEG (Fig. 1). An electrical potential representing the dipole strength can be measured at scalp as the voltage difference between two different recording sites, with one site serving as the reference for the other (e.g., in Fig. 1A, site E2 is used as reference for site E1, resulting in a negative potential measurement for a current dipole with its negative pole directed towards site E1). The absolute value of this measured potential has no physical meaning (e.g., Nunez and Srinivasan, 2006), other than representing the potential difference between the two recording sites. Thus, if the same dipole is measured at the same two scalp locations but after reversing the assignment of 'active' and reference site, a positive potential measurement is obtained (Fig. 1B). Other than the reversal in sign, this positive potential has the same absolute value as the previously measured negative potential, and both measurements are equally valid representations of the underlying current dipole. Moreover, the *direction* (or sign) of the *relative* difference between the two recording sites is entirely unaffected by selecting either one as the reference (i.e., $E1 - E2 = -[E2 - E1]$).

We further note that no potential is measured between any two sites if the dipole orientation and location affects both recording sites equally (e.g., both sites are located on the same isopotential line), regardless of dipole strength. Of course, a zero potential is also measured if there is no underlying dipole. Importantly, because no *inactive*, *silent*, *quiet* or *infinite* recording site exists anywhere on body (cf. Nunez and Srinivasan, 2006; Kayser and Tenke, 2010), the choice of using one recording site as the reference for another is inherently arbitrary, and this arbitrariness is not resolved by employing a consensus for an EEG reference (i.e., nose, linked-mastoids or -ears, and average reference are commonly used).[1] EEG measures, or surface potentials (SPs), cannot be understood in isolation from their reference.

[1] There are perfectly good reasons for utilizing a particular EEG reference, such as providing a conventional standard that allows for easy comparisons across studies or the desire to emphasize some feature of brain activity which may be less clear or obscured with a different reference (e.g., Dien, 1998). However, these considerations do not alter the conceptual ambiguity of surface potentials as universal indicators of brain activation.

These basic principles equally apply to multichannel EEG montages, although their implications become more complicated with an increasing number of recording sites and simultaneously active dipoles, which change in time and space. The impact of choosing a different reference for ERP data obtained with an extended 10–20 system 67-channel EEG montage is illustrated in Fig. 2, which directly compares three common reference schemes: a nose reference (NR), a linked-mastoids reference (LM; average of sites TP9 and TP10), and an average reference (mean ERP activity across all 67 sites; cf. Supplementary Fig. S1 for ERP waveforms plotted separately for each reference at 10–20 system sites, including their comparisons at midline sites). These ERPs were recorded from 44 healthy adults during a visual continuous recognition memory task employing foveal presentations of common English nouns or black-and-white photographs of unknown faces (for further details, see Kayser et al., 2010). Depending on the reference scheme, the resulting waveforms differ dramatically in their sequence of prominent deflections at any given scalp location, affecting their peak amplitude, peak latency and peak location. For words, for example, the NR data at site T8 show two consecutive negative ERP deflections peaking at 200 and 330 ms, followed by a robust positive deflection peaking at 600 ms. At the same site, the LM data show a small negative deflection peak at 90 ms, followed by a positive peak at 145 ms and a late positivity peaking at 900 ms. The AR data, however, reveal only a negative ERP deflection at T8 peaking at 215 ms but no substantial late negativity or positivity. As another example, for faces, NR and AR data show early positive–negative ERP deflections at site P04, peaking at 90 and 150 ms, respectively, whereas this peak sequence is virtually absent in the LM data, which shows no negative deflection at 150 ms at all. Beyond 300 ms, however, NR and LM data appear to have almost identical waveforms for faces at PO4, with a common positive maximum at 600 ms, whereas AR data has a positive maximum at 290 ms. Similar discrepancies can be observed at any given site (e.g., cf. insets for PO4 in Fig. 2A and for T8 in Fig. 2B).

In contrast to a linked-mastoids and average reference, the nose reference represents a single reference location, resulting in an ERP waveform that is zero at all sample points (flat green lines at Nose insets in Fig. 2). This provides an excellent opportunity to visualize the impact of the reference for the ERP signal at all other sites, keeping in mind that the same principle applies to *all* references, not just the nose reference. Rereferencing the NR waveforms to the mean of TP9 and TP10 (LM) or of all recording sites (AR) means this new reference waveform is subtracted from all 67 recording sites. Thus, the inverted LM and AR reference waveforms are revealed at the Nose site (red and blue lines), indicating that substantial and complex ERP activity is removed from the nose-referenced ERPs, and that this removed ERP activity is highly specific to the particular reference scheme. Furthermore, by comparing these inverted reference waveforms for words and faces (Nose insets in Fig. 2A and B), it becomes obvious that NR and AR

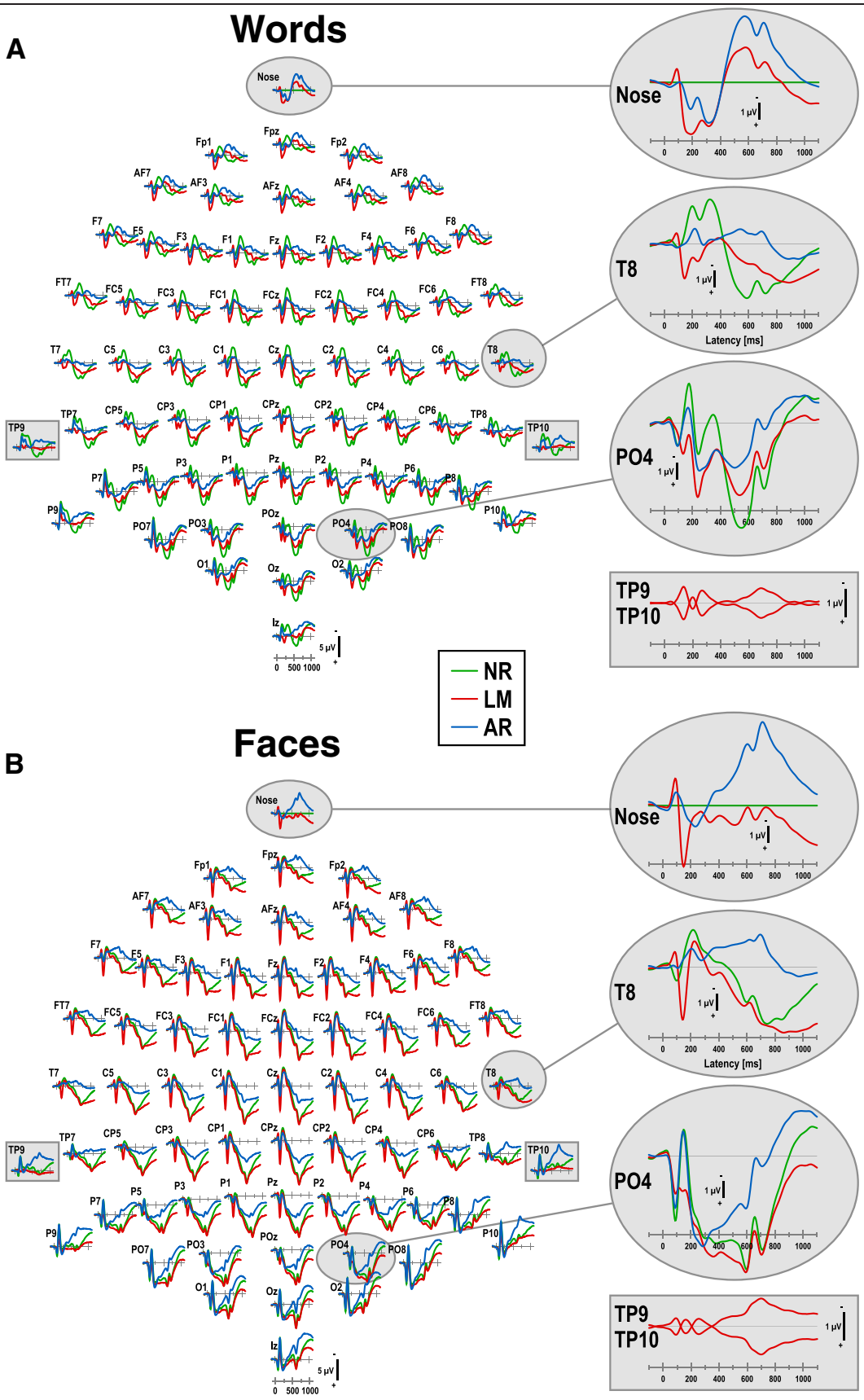

Fig. 2. Impact of the EEG reference (NR: nose reference; LM: linked-mastoids reference; AR: average reference) on grand mean ($N = 44$) ERP [µV] waveforms (−100 to 1100 ms, 100 ms pre-stimulus baseline) to foveal presentations of common words (A) or unknown faces (B) recorded during a continuous recognition memory task (data of healthy adults from Kayser et al., 2010). Enlargements of selected sites are shown on the right to highlight the substantial differences in ERP waveforms between references, although these can be observed at all sites. Rectangle enlargements directly compare ERPs referenced to linked mastoids at sites TP9 and TP10 (i.e., left and right mastoid), revealing symmetric activity with opposite polarity.

reference waveforms also depend uniquely on these two stimulus types (and by extension on task, paradigm, condition, modality, response requirements, etc.).

A special case would be the LM ERP waveforms at the very same sites that were used to compute the linked-mastoids reference (i.e., TP9 and TP10; rectangular insets in Fig. 2). By removing the algebraic mean from either site, the resulting reference ERPs become inverted waveforms of each other (symmetric ERPs with respect to the baseline). However, ERP deflections that are common to both sites with any other reference are completely removed from TP9 and TP10, similar to the flat line seen at the Nose for NR data. Notably, this reference effect is less obvious for the LM data because it is masked by the residual waveforms remaining at these sites.

It is easy to see how using a different EEG reference will lead to different ERP analyses and findings. A researcher may focus on the 'obvious' ERP deflections, be inclined to label them according to their polarity, peak latency and peak locations, measure certain characteristics (e.g., baseline-to-peak or integrated amplitude, peak latency), perform a statistical test, and refer to them as ERP components. However, as illustrated in Fig. 2, this analytic strategy is misguided because the underlying neuronal generator activity has not been changed by rereferencing surface potentials. Even employing a multivariate data analytic approach will not resolve the ambiguity of when and where the ERP deflections are, because these approaches rely on the variance structure of the data, which is directly affected by the choice of reference. For example, principal components analysis (PCA) is often used for ERP analysis, with temporal, spatial or spatiotemporal PCA being fairly common (e.g., Barry and De Blasio, 2013; Kayser and Tenke, 2003; Spencer et al., 2001; van Boxtel, 1998). For a covariance association matrix, a common choice for factor extraction, the PCA identifies the variance structure by removal of the grand mean (i.e., the variance around the grand mean), which differs for every EEG reference. Thus, regardless of erroneous claims in the literature, a PCA or any other multivariate procedure that depends on data variance or absolute values does not constitute a reference-free approach (i.e., it will yields different results depending on the EEG reference).

But what about the average reference (e.g., Lehmann and Skrandies, 1980)? It has been argued that if the volume that generates the electrical signal (i.e., the brain case) is measured at many different surface locations and from all directions (i.e., by using a high-density EEG montage of 128 or more channels), the sum of the recorded EEG activity will approximate zero, and therefore, the average of this activity will approximate an inactive reference (e.g., Bertrand et al., 1985). A related argument pertains to the requirement of inverse solution algorithms that the net source activity within the brain sums to zero at each measurement (sample) point (e.g., Murray et al., 2008). Of course, given the lack of surface area, it is not possible to place EEG electrodes ventrally to the brain case, thereby rendering this theoretical requirement a practical impossibility. Another issue that arises from using an EEG reference computed from the measures obtained at all scalp locations is that it will vary with each EEG montage, depending on the montage density and specific scalp locations used. In any case, however, the computed average reference is, like any other reference scheme, a single value (constant) that is subtracted from the values obtained at each recording site for each measurement point (e.g., a fixed waveform in case of ERPs).

Despite the ambiguity of reference-dependent surface potentials, which yield different EEG waveforms for each recording site depending of the chosen reference, the *relationship* between signals in an EEG topography is fixed. This is a direct consequence of the principle described above (Fig. 1), that is, the relative difference between two recording sites is unaffected by the choice of the recording reference (e.g., Osselton, 1965). For this reason, the difference between any two ERP waveforms in a given EEG montage is exactly the same for a nose, linked-mastoids or average reference, regardless of their uniquely different ERP waveforms at either site (Fig. 3). By extension, this reference-independent relationship of EEG activity recorded at different scalp sites is also true for ERP difference waveforms (i.e., between conditions or groups). However, condition (or group) differences at specific sites are also affected by the choice of reference (cf. column 3 in Fig. 3, showing faces-minus-words ERP difference waveforms as an example). This characteristic relationship between EEG activity at different recording locations (i.e., topography) is both unique (i.e., there is only one difference between any two sites) and reference-free, and it is at the core of the surface Laplacian.[2]

1.2. What is a surface Laplacian transform?

The biophysical principle of volume conduction relates current sources generated within the brain to the macroscopic potentials observable at scalp according to Poisson's equation (e.g., Carvalhaes and de Barros, 2015; Nunez and Srinivasan, 2006; Tenke and Kayser, 2012). A surface Laplacian (often also termed Laplacian, scalp current density [SCD], current source density [CSD]), is a mathematical simplification of this equation as a vector form of Ohm's law, relating current generators within an (isotropic) electrical conductor to the (negative) second spatial derivative of the field potential at each electrode.[3] To help understanding what this means, let us consider a series of values at discrete locations labeled A-I, with locations spreading in a single direction and separated by an equal amount of distance (Fig. 4). In this scenario, we may conceive this data series as a numerical function, which can be characterized by its instantaneous change in amplitude that is equal to the slope of a tangent line at each data point (first derivative = differences between neighboring points = gradient). Repeating this operation on the resulting data series (second derivative = differences of these differences), and inverting these secondary slopes, yields a data series that reflects the rate of change in slope across the observed original values. As shown in Fig. 4, despite a nominal maximum of the original values at location E (green line), the change rate in slope was notably larger at locations C and G (red line), because site E has neighboring sites of similar amplitude (sites D and F).

It is also intuitively obvious from Fig. 4 that subtracting the value measured at location E from all other sites (the equivalent of rereferencing the data series to site E) will merely shift the original data series without changing its shape. Therefore, its first and second derivative will remain the same. This further indicates that the sign (or polarity) of the second derivative is not affected by the subtraction of a constant (or referencing the data), in contrast to the original data. Although less obvious, Fig. 4 also reveals another characteristic of this data transformation: larger changes in amplitude at neighboring sites are enhanced when compared to the original data, which has been described as a signal 'edge detection' feature.[4]

The above example illustrates the principle of a Laplacian transformation for a one-dimensional scenario, which is often employed in intracranial EEG studies (cf. Tenke and Kayser, 2012). For a linear

[2] The uniqueness of an EEG topography is also at the heart of any inverse solution (e.g., Michel et al., 2004), such as low resolution brain electromagnetic tomography (LORETA; Pascual-Marqui et al., 1994) or brain electrical source analysis (BESA; Scherg and von Cramon, 1985), rendering these likewise reference-free transformations; unlike the surface Laplacian, however, inverse solutions are non-unique.

[3] It is important to distinguish between an analytic SL, which is a theoretical estimate usually obtained with forward simulations (e.g., Babiloni et al., 1996; Nunez, 1981; Nunez and Srinivasan, 2006), and various empirical estimates of this variable, which include spherical spline interpolations (e.g., Carvalhaes and de Barros, 2015). Likewise, the term CSD has also been used in other contexts, including laminar intracranial recordings from cortical depths arrays or inverse solutions (e.g., LORETA), which has resulted in considerable confusion (a historical context of the EEG surface Laplacian by Paul L. Nunez is available at *http://ssltool.sourceforge.net/history.html*). Here, we are referring exclusively to scalp SL estimates.

[4] Using the term 'edge detection' may incorrectly reduce the SL transform to a mere pattern recognition algorithm. However, the surface Laplacian, being directly derived from Poisson's equation, represents a physiologically meaningful data transformation, as it provides a concise simplification of a field topography (e.g., Nunez and Srinivasan, 2006; Tenke and Kayser, 2012).

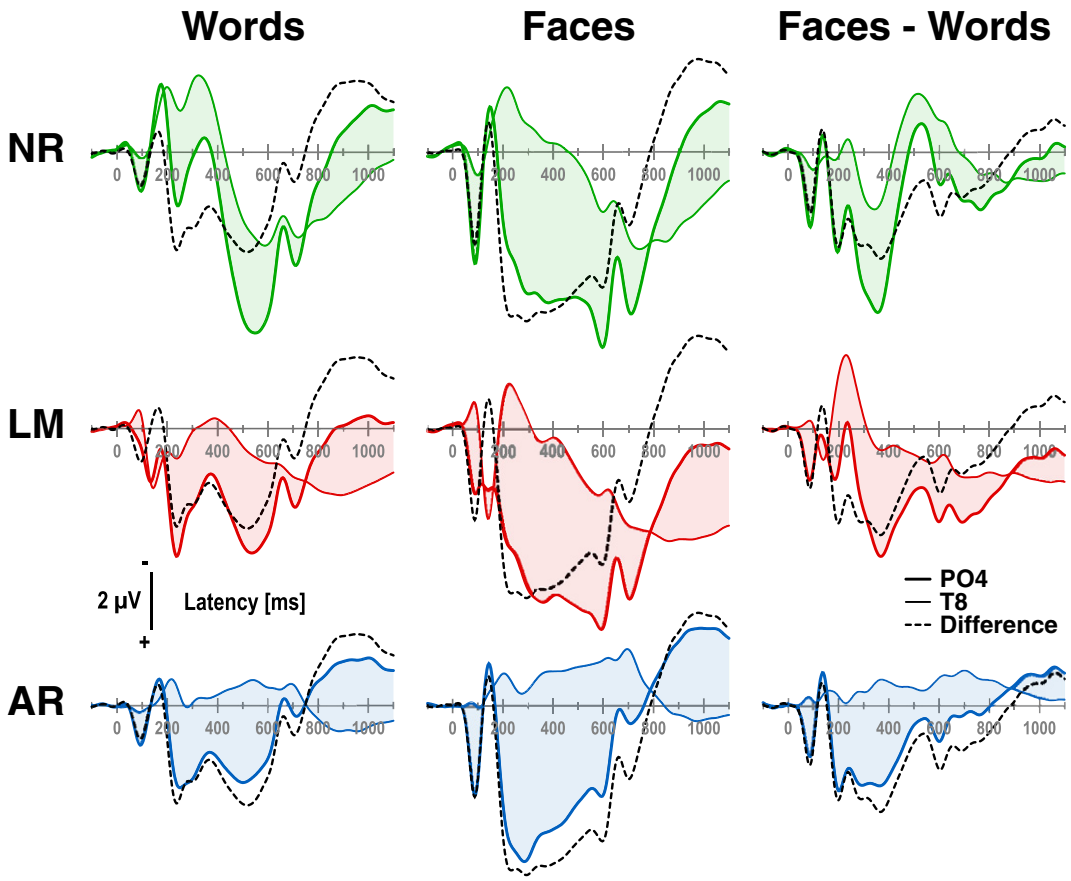

Fig. 3. Selected ERP waveforms (colored lines, PO4: thick, T8: thin) for words (column 1) and faces (column 2) as shown in Fig. 2, and ERP difference waveforms (i.e., faces-minus-words; column 3), comparing three common EEG references (NR: nose reference; LM: linked-mastoids reference; AR: average reference; colors as in Fig. 2). The shaded areas and the black dashed lines depict the differences between the two ERPs shown in each subgraph (i.e., thick-minus-thin colored lines). Relative ERP differences between any two sites are unaffected by the EEG reference, as revealed by identical difference waveforms in each column (dashed lines). It is obvious that any attempt to quantify deflections (i.e., peak and troughs) of the colored lines will yield different results for each EEG reference, notwithstanding their invariance in topography across references.

penetration of tissue, Freeman and Nicholson (1975) originally proposed a local "slope-of- slope" measure as applied in Fig. 4, but simplified the computation as the potential at each electrode minus half of

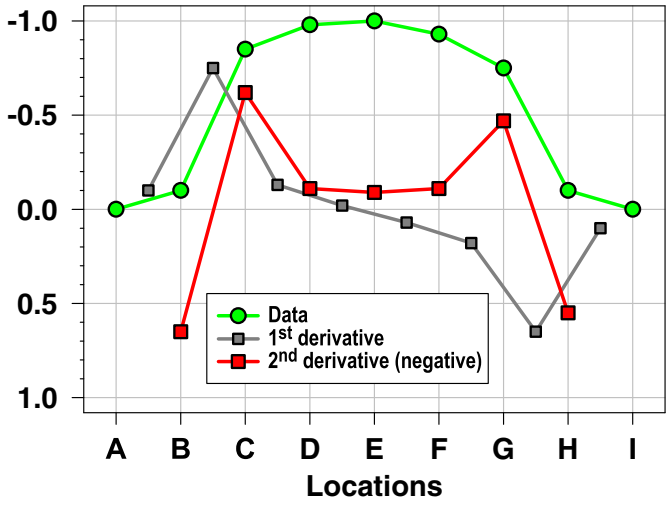

Fig. 4. First and (negative) second (spatial) derivatives of a data series measured at one time point (sample) across nine (scalp) locations (labeled A-I), with negative values plotted upwards. The resulting differences between consecutive data points (1st derivative) are plotted half-way between locations (gray squares). Analogously, the resulting (negative) differences between consecutive difference values (2nd derivative) are plotted half-way between these intermediate locations (i.e., the middle of a 3-point computation; red squares).

the potentials at each of the two neighboring sites. Local smoothing can be obtained by expanding this algorithm to the four nearest neighbors and weighting the subtracted potentials by distance.[5]

An extension of this nearest-neighbor algorithm from one-dimensional data arrays to two- dimensional surfaces is the local Hjorth (Hjorth, 1975, 1980). Here, an estimate of the second spatial derivative is likewise computed by subtracting the potentials of all neighboring sites weighted by their inverse distance from the potential measured at a given location. This requires the designation of a differentiation grid for a given EEG montage (i.e., the number and location of neighbors for each recording site), with number of nearest neighbors typically varying between 3 and 5 (cf. also Eq. (1) and Fig. 1 in Tenke et al., 1998), although any number of 'nearest' neighbors (up to n-1recording sites) can be defined. Fig. 5 shows a 3–5 nearest neighbor local Hjorth grid for the 67-channel EEG montage shown in Fig. 2. In this case, for example, the surface Laplacian at site Cz is estimated from the surface potentials measured at Cz and its four nearest neighbors (C1, C2, FCz, CPz). Given that these neighbors have all the same distance d to the site Cz, owing to the fact that these are standard 10–10 system locations (e.g., Jurcak et al., 2007), the surface Laplacian (local Hjorth H) at site Cz is computed from the observed potentials P as $H_{Cz} = P_{Cz} - (P_{C1}/d + P_{C2}/d + P_{FCz}/d + P_{CPz}/d)/4d = P_{Cz} - (P_{C1} + P_{C2} + P_{FCz} + P_{CPz})/4$. Accordingly, the local Hjorth derivation for the entire 67-channel EEG montage can be conveniently defined via a channel-by-channel

[5] A hybrid approach was suggested by Tenke et al. (1993), whereby the application of multiple differentiation grids (e.g., both nearest-neighbor and next-nearest-neighbor 3-point calculations) could improve the interpretability of high-resolution data.

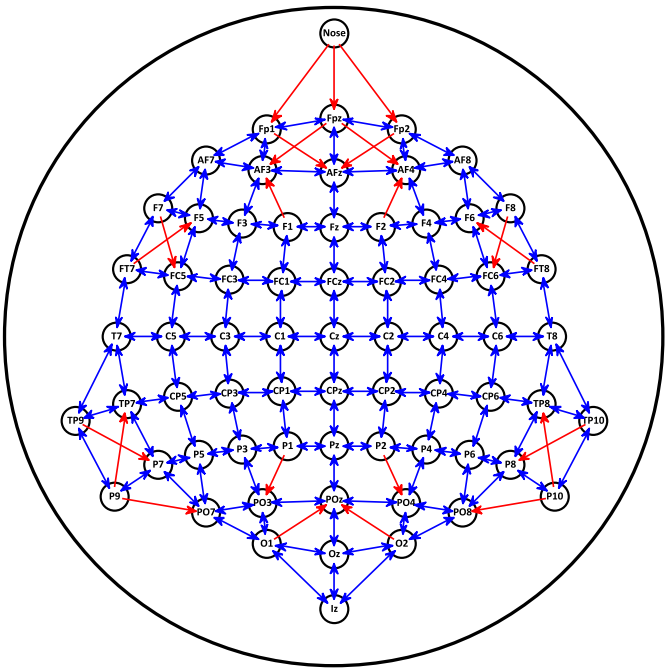

Fig. 5. Local Hjorth differentiation grid consisting of 3–5 nearest neighbors for a 67-channel EEG montage (cf. Fig. 2). Mutual and single (one-directional) neighbors are marked by blue and red arrows for each scalp site.

transformation matrix, with the diagonal consisting of ones (+1.0) and the other columns in each row representing the respective (negative) weights for each neighboring site, or zeros if not included in the set of nearest neighbors for a given site; the local Hjorth estimates simply corresponds to the rowwise sums of the potentials measured at each site multiplied by the column weights (an analogous formalization can be easily defined in the one-dimensional case via a transformation vector). Because this transformation matrix is independent of the actual EEG signal (i.e., the values obtained for each recording site), it only needs to be defined once for a given montage, and can then be applied to any time point of any EEG data set employing this montage.

Fig. 6 compares N1 and P3 ERP topographies (using waveform peak amplitudes of visual word stimuli shown in Fig. 2A) with their surface Laplacian estimates stemming from this 3–5 nearest neighbors local Hjorth montage, as well as three additional local Hjorth differentiation grids using 8–9, 24–25 or 66 (i.e., all) nearest neighbors. Although overall amplitude and polarity of the ERP measures at each recording site differ substantially across different EEG references (Fig. 6A), their N1 and P3 topographies remain the same, revealing a negative maximum for N1 over left inferior-parietal sites and a positive maximum for P3 over mid-parietal sites.[6] Consequently, these ERP topographies (NR, LM, AR, or any other reference scheme) will render identical local Hjorth estimates for any given differentiation grid (Fig. 6B). Depending on the number of nearest neighbors, the representation of surface potentials gradients will be more or less abrupt, with smoother transitions for increasing numbers of nearest neighbors. Whereas volume conduction results in smoother (or smeared) surface potential topographies, stretching any local minimum or maximum to neighboring scalp locations (cf. isopotential lines in Fig. 6A), the topographic pattern is markedly sharper for local Hjorth estimates, particularly for those based on fewer nearest neighbors, yielding a more focal left-lateralized N1 and a more constrained mid-parietal P3. Less accurate surface Laplacian estimates are obtained for locations around the edge of the EEG montage, where fewer neighbors are available, thereby preventing a symmetric sampling of the field around each site. However, these adverse effects are notably mitigated when including additional (up to all 66) nearest neighbors, which is equivalent to the smoothing effect in the one-dimensional case by widening the differentiation span. While employing many 'nearest' neighbors may be counterintuitive, seemingly upending the purpose of a local Hjorth, the impact or weight for signal differentiation will nevertheless be greater for the immediate neighbors compared to those at more distant locations (i.e., any subtracted potential is scaled by the inverse of its distance).

Given the nature of the second spatial derivative, the calculation of the surface Laplacian is not directly affected by temporal signal properties (i.e., the SL estimate at time point t is not impacted by the SL estimates at t - 1 or t + 1), in contrast to temporal filters. However, because EEG time series data are highly intercorrelated, SL estimates for consecutive time points will also be similar (i.e., the surface Laplacian does not impose independence on time-correlated data). Furthermore, because the transformation itself is a linear operation, it will not interfere with other linear data transformations, including averaging the EEG across epochs (trials) or subjects, baseline correction, and applying a temporal filter (i.e., these transformations may be applied to the EEG data either before or after the surface Laplacian transform without altering the final result). Importantly, this rule does not hold for any nonlinear transformation, including the computation of spectral estimates (power) that involves rectifying (squaring) the data (cf. Fig. 1 in Tenke and Kayser, 2005). For this reason, all nonlinear operations have to be performed on the CSD-transformed data (i.e., *after* the surface Laplacian transform).

[6] For the linked-mastoids reference, the overall N1 topography is heavily biased towards positive values, which may tempt a researcher to focus on a broad midfrontal positivity during this time period and interpret these data in terms of a positive ERP component. Such an erroneous bias becomes even more likely when a less dense EEG montage is used, or by adopting a 'region-of- interest' approach that isolates a selected subset of 'representative' recording sites. A related example is the inversion of a face-sensitive N170 between inferior lateral parieto-occipital sites and Cz, where the use of different EEG references has given rise to a 'separate' component termed vertex positive potential (VPP; e.g., Joyce and Rossion, 2005).

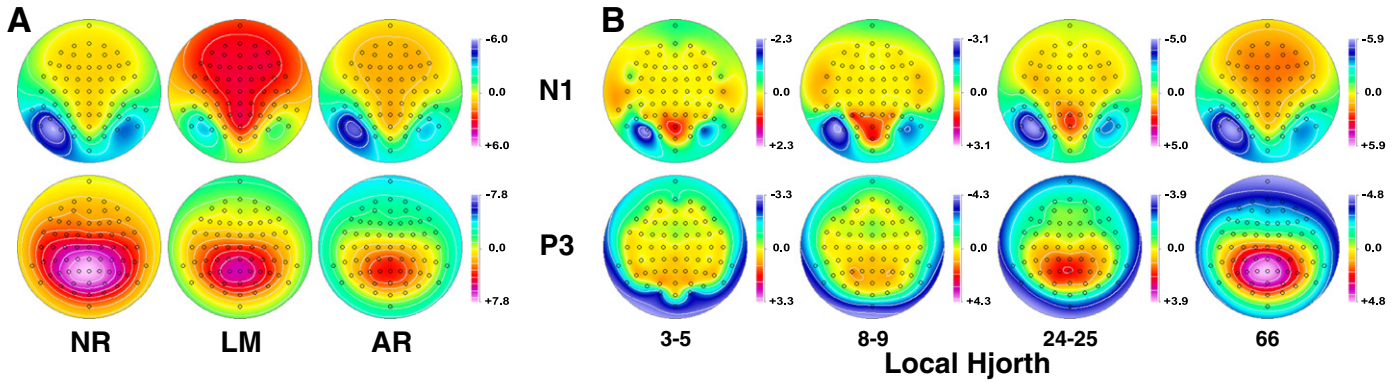

Fig. 6. (A) Topographies of grand mean ERPs [μV] to word stimuli (Fig. 2A) at the peak latency for N1 (144 ms) and P3 (560 ms) referenced to nose (NR), linked mastoids (LM) or the average of all 67 sites (AR). (B) Local Hjorth estimates of these N1 and P3 topographies using differentiation grids consisting of 3–5 (cf. Fig. 5), 8–9, 24–25 or 66 nearest neighbors. All topographies were created from the ERP or local Hjorth values at each sites using a spherical spline surface Laplacian interpolation ($m = 2$; $\lambda = 0$; Perrin et al., 1989).

1.3. Surface Laplacian estimation via spherical splines

An obvious limitation of the local Hjorth is that the second spatial derivative is derived from a discrete differentiation grid, impeding estimates not only at the edge of the EEG montage but at any given site, as estimates depend on the number and location of nearest neighbors. These adverse effects are compounded by the characteristics of the EEG montage, namely electrode density and spacing uniformity. However, signal interpolation can be used to overcome these deficiencies. Several algorithms have been proposed for smooth EEG surface reconstruction and surface Laplacian estimation (Carvalhaes and Suppes, 2011; Nunez and Srinivasan, 2006), ranging from local polynomial estimates (e.g., Wang and Begleiter, 1999) to global spline interpolations using a simple spherical (e.g., Carvalhaes and Suppes, 2011; Gevins, 1996; Nunez and Westdorp, 1994; Nunez et al., 1994; Perrin et al., 1987, 1989; Pascual-Marqui et al., 1988; Srinivasan et al., 1996, 1998a) or increasingly realistic scalp surface head models (e.g., Babiloni et al., 1995, 1996, 1997; Bortel and Sovka, 2007, 2013; Gevins et al., 1999; He et al., 2001; Law et al., 1993a; Yao, 2000, 2002a). A popular choice among these surface Laplacian techniques is interpolation via spherical splines, as proposed by Perrin et al. (1989).

1.3.1. Spline flexibility

Spherical spline functions are used to fit the observed data at each recording site and can then provide a continuous projection of the (missing) data at any (intermediate) surface location.[7] A fundamental characteristic of these functions is spline flexibility, that is, the degree to which these functions can be bent to best fit the actual data, which affects the smoothness of the continuous interpolation. Spline flexibility is determined by a constant m, which is an integer value greater than 1 (e.g., Carvalhaes and Suppes, 2011; Perrin et al., 1989; cf. Eq. (2) in Kayser and Tenke, 2006a). The most flexible spline function corresponds to $m = 2$, and increasingly more rigid splines correspond to greater values of m. The top panel of Fig. 7 illustrates the effects of spline flexibility for the interpolation of the above data series for the hypothetical locations A-I (cf. Fig. 4) under the additional assumption that these equidistant locations are located on the surface of a sphere. Whereas the most flexible splines of $m = 2$ and $m = 3$ (red and green lines) directly or approximately intersect with the observed data points (green circles), this is not necessarily the case for splines of intermediate ($m = 4$, blue) or reduced ($m = 5$, orange) flexibility. At the same time, less flexible splines provide increasingly smoother estimates, and all spline interpolations provide estimates for intermediate locations and those beyond the borders of the array. Consequently, the (negative) second spatial derivatives corresponding to these spherical spline interpolations (Fig. 7, bottom) represent continuous surface Laplacian estimates, which provide appropriate gradient transitions across locations, being sharper and enhanced for more flexible splines but smoother and more gradual for less flexible splines. The shapes of these spline-based surface Laplacian estimates (with the exception of $m = 5$) are similar to that of the discrete second spatial derivative (Fig. 4), and all spline-based surface Laplacian estimates are also reference-free (i.e., invariant to the addition of a constant to the data series).

As with the local Hjorth algorithm, the surface Laplacian estimate at any recording site (or intermediate surface location) depends only on the data measured at that site in relation to the potentials measured all other sites (i.e., the 'neighbors'), with their impact weighted by their (spherical) distance to the site (surface location) under consideration. Thus, while *all* recording sites affect the surface Laplacian estimate at *any* surface location, their influence will depend on the *specific* surface location. In fact, for a given spline flexibility (and other fixed computation parameters discussed below), the (spherical) distances between the to-be-estimated CSD location and all EEG recording sites are the sole determinants for computing the CSD estimate from the surface potentials. Because all electrode sites are assumed to be on the scalp surface and the scalp is modeled as a sphere, the distance (in mm) between electrode locations is proportional to their angular distance, which is readily expressed by the cosine of the angle between any two surface points (i.e., radians). For example, for a unit sphere (radius $r = 1$), the spherical distance between T7 and T8 equals π (i.e., 180° or half the circumference of a great circle), π/2 between

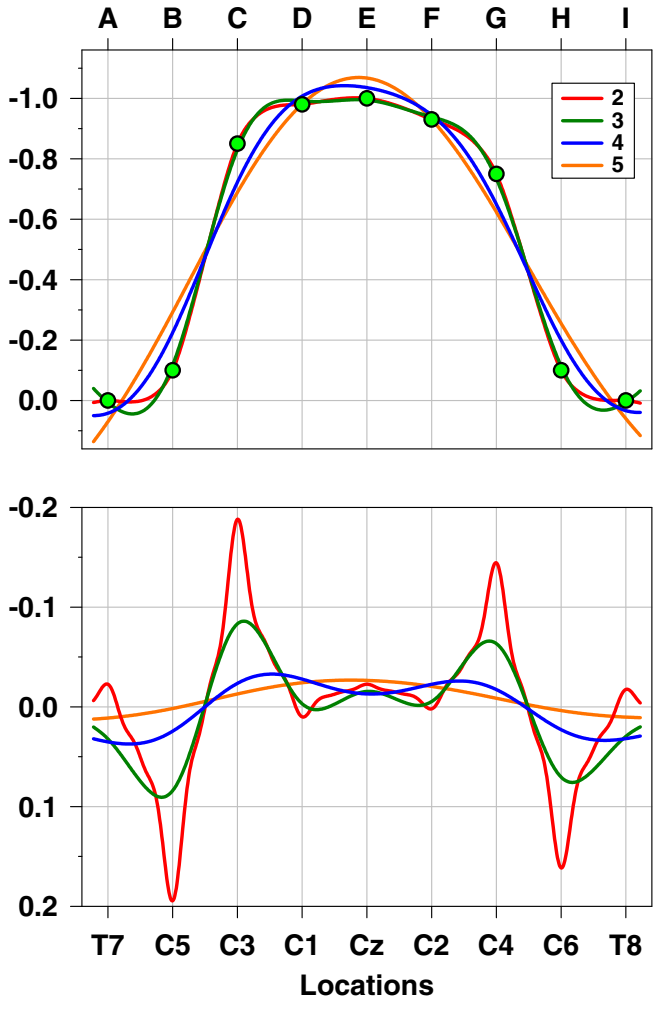

Fig. 7. Data interpolation of discrete data values (green circles, top panel; cf. Fig. 4) and corresponding surface Laplacian estimates (negative second spatial derivative, bottom panel) using spherical splines of different flexibility ($m = 2$–5; $\lambda = 10^{-5}$; Perrin et al., 1989). Because the equivalent spacing of the 9 locations labeled A-I is identical to the scalp surface distances of 9 positions in the coronal plane of the 10–10 system, ranging from T7 to T8 (Jurcak et al., 2007), the hypothetical data series may be conceived as an ERP topography having a negative maximum at vertex (e.g., N1 peak at Cz), with corresponding units of μV (surface potential) and μV/cm^2 (surface Laplacian).

[7] This is also the method of choice to interpolate artifactual data at affected sites, which can be applied for an entire recording session or a shorter interval (e.g., a trial epoch). In this case, the interpolation estimate is derived from the available (i.e., artifact-free) data recorded at all other sites. Therefore, the validity of the estimates depends on the number of artifact-free sites, their data quality (i.e., signal-to-noise ratio), and appropriateness of the chosen spline computation parameters.

T7 and Cz (90°), or π/8 between T7 and C5 (i.e., 90°/4).[8] It is therefore of critical importance to correctly assign the measured surface potentials to their (approximate) surface location, applying either a template for standard 10–20 system locations (and its 10–10 and 10–5 extensions; cf. Jurcak et al., 2007; Oostenveld and Praamstra, 2001) or specifying locations via any coordinate system for three-dimensional space (Cartesian, polar, spherical), all of which can be easily converted to reflect unit sphere surface locations.

Given that locations A-I (Fig. 7) were assumed to represent equally-spaced sites on the surface of a sphere, they may be directly used to represent known scalp locations, such as those marking the coronal plane of the 10–10 system (e.g., Jurcak et al., 2007) from the left lateral temporal (T7) through vertex (Cz) to right lateral temporal (T8). In this scenario, the 'observed' negative surface potential maximum at Cz, its gradual fall-off towards mid-central sites (C3/4) and steep decline towards temporal sites (T7/8) approximate a typical auditory N1 ERP topography, which has a negative maximum over mid-frontocentral sites at about 100 ms post stimulus onset (e.g., Näätänen and Picton, 1987). Fig. 8A shows a complete typical auditory N1 topography for a 72-channel EEG montage (average reference) and the corresponding surface Laplacian (CSD) estimates using spherical splines of different flexibility ($m = 2 . 5$). Although the ERP N1 maximum is at FCz, Cz shows the most negative value across the nine centrotemporal sites (marked as gray circles in Fig. 8A). Similarly, overall N1 minima (most positive values) are bilaterally at inferior temporal-parietal sites (TP9/10 or mastoids), but at T7 and T8 when considering only these centrotemporal sites (i.e., the measured potentials are consistent with the data series depicted in Figs. 4 and 7). Likewise, the corresponding surface Laplacian estimates at these sites, although being integrated in an overall CSD topography, basically reiterate the surface Laplacian spline patterns across these sites (cf. Fig. 7, bottom), showing sharper and enhanced transitions for more flexible splines but a smoother and more gradual distribution for more rigid splines.[9]

The same relation between spline flexibility and SL smoothness can be observed for the CSD topographies corresponding to the visual N1 (Fig. 8C), which are highly comparable to the local Hjorth transformations using a different number of nearest neighbors (Fig. 6B). This is also true for the visual P3 (Fig. 8D), where the overall activation pattern is consistent across spline flexibilities; however, its broad scalp distribution becomes discontinuous with more flexible splines ($m = 2$–3).

Importantly, all CSD topographies are reference-free estimates of radial current flow at scalp, their sign (polarity) reflecting the direction of radial current flow with respect the scalp surface (positive values or sources represent current flow towards the scalp, negative values or sinks represent current flow exiting the scalp; e.g., Nunez, 1981; Nunez and Srinivasan, 2006). For this reason, the CSD pattern of sources and sinks provides a representation of current generators underlying an ERP topography (e.g., Tenke and Kayser, 2012), which can be obtained from *any* EEG recording reference scheme. In case of the auditory N1, the underlying current generator pattern consists of bihemispheric dipole activity involving both auditory cortices, which can be readily appreciated from the CSD topographies, particularly for those with intermediate spline flexibility ($m = 3$ or $m = 4$). In contrast, this pattern is blurred for surface potentials, resulting in a diffuse midline maximum. Furthermore, despite preserving the relative topographic distribution of ERP values when using different reference schemes, in case of the auditory N1, a linked-mastoids reference will largely eliminate positive values across the recording montage, which may further mask the underlying bihemispheric activation pattern. Another important observation is that the CSD topographies clearly reflect the well-known anatomical differences between the two hemispheres, involving asymmetries of the planum temporale posterior to Heschl's gyrus (primary auditory cortex) within the Sylvian fissure (e.g., Galaburda, 1995; Geschwind and Levitsky, 1968; Witelson and Kigar, 1988), which affect both location and orientation of the neuronal generators underlying auditory N1.

1.3.2. Montage density

As noted above, montage density is another critical consideration for EEG data, affecting surface potential and surface Laplacian estimates alike. Dense electrode arrays (64 or more electrodes), affording whole head coverage with interelectrode distances below 2 cm, are generally preferred to a low-density EEG montage (less than 21) with interelectrode distances greater than 6 cm (e.g., Nunez and Srinivasan, 2006). The effect of reducing the spatial sampling from 72 to 31 scalp locations for an auditory N1 topography is shown in Fig. 8B. The average reference, now based on fewer sites, is slightly altered, as can be inferred from the isopotential contour lines. CSD estimates are also affected, resulting in the unsystematic removal of higher spatial frequencies from the signal (i.e., spatial integration). This effect is most noticeable for more flexible spline interpolations (correlations between 72- and 31-channel topographies across 80381 surface points, for $m = 2$, $r = 0.5954$; for $m = 3$, $r = 0.8916$), whereas less flexible splines largely retain the 72-channel topography (for $m = 4$, $r = 0.9752$; for $m = 5$, $r = 0.9754$). Thus, spline flexibility acts as a spatial filter that can be optimized to enhance the signal of interests, for example, by choosing a less flexible spline for ERP studies in the time domain aimed at group and/or condition comparisons (e.g., Kayser and Tenke, 2006a, 2006b; Law et al., 1993b), or a more flexible spline for studying individual EEG coherence in the frequency domain (e.g., Nunez et al., 1997, 1999; Srinivasan et al., 1998a).[10] However, a low-density EEG montage will itself impose a spatial low pass filter (e.g., Srinivasan et al., 1998b; Tucker, 1993).

1.3.3. Spline regularization

It is generally desirable to improve the signal-to-noise ratio of surface Laplacian estimates, which can be seriously compromised by EEG/ERP recording noise (e.g., Babiloni et al., 1995). To counteract this problem, a regularization parameter is used to smooth the interpolated surface potentials prior to the computation of the surface Laplacian (e.g., Nunez and Srinivasan, 2006). For the spherical spline surface Laplacian estimates, this smoothing constant has been termed lambda λ (Perrin et al., 1989). Comparing the effects of various spline orders ($m = 2$–5), montage densities (28 to 256 scalp sites), and spatial frequencies of noise (0.05 to 0.23 cycles/cm), Babiloni et al. (1995) found that spline flexibility strongly influenced the optimal choice for λ (i.e., greater spline flexibility required greater smoothing, with optimal values of $10^{-9} \leq \lambda \leq 10^{-2}$), indicating that λ correction also acts as a spatial filter. By comparison, spatial noise and montage density had only moderate impact for determining optimal values for λ. Importantly, λ correction significantly improved spherical spline surface Laplacian estimates when compared with the 'analytic' surface Laplacian distribution, which was directly computed from the (mathematically) simulated surface potentials (Babiloni et al., 1995).

[8] Radians were also used as distance measures for the computation of local Hjorth estimates.

[9] When comparing Fig. 8A with Fig. 7 (and also Fig. 4), it is important to keep in mind that the data of Fig. 7 represent a 1-D simplification of a 3-D surface void of the additional measures available at anterior and posterior sites. Thus, while the interpolations in Fig. 7 are optimal for the limited data array, any localization of the "real" sources near TP9 and TP10 will necessarily require the additional spatial dimension.

[10] The surface Laplacian routinely employed by Nunez and associates (New Orleans spline Laplacian algorithm) is based on surface potential interpolation in three-dimensional space, and computes the two-dimensional surface Laplacian by subtracting the second spatial derivative in radial direction (cf. Appendix J in Nunez and Srinivasan, 2006; Matlab toolbox developed by Siyi Deng, version 1.4b beta, downloaded 17-Oct-2014 at http://ssltool.sourceforge.net/index.html). This algorithm yields CSD estimates comparable to those obtained with flexible spherical splines ($m = 2$ or $m = 3$, depending on the specific spline smoothing or regularization parameter).

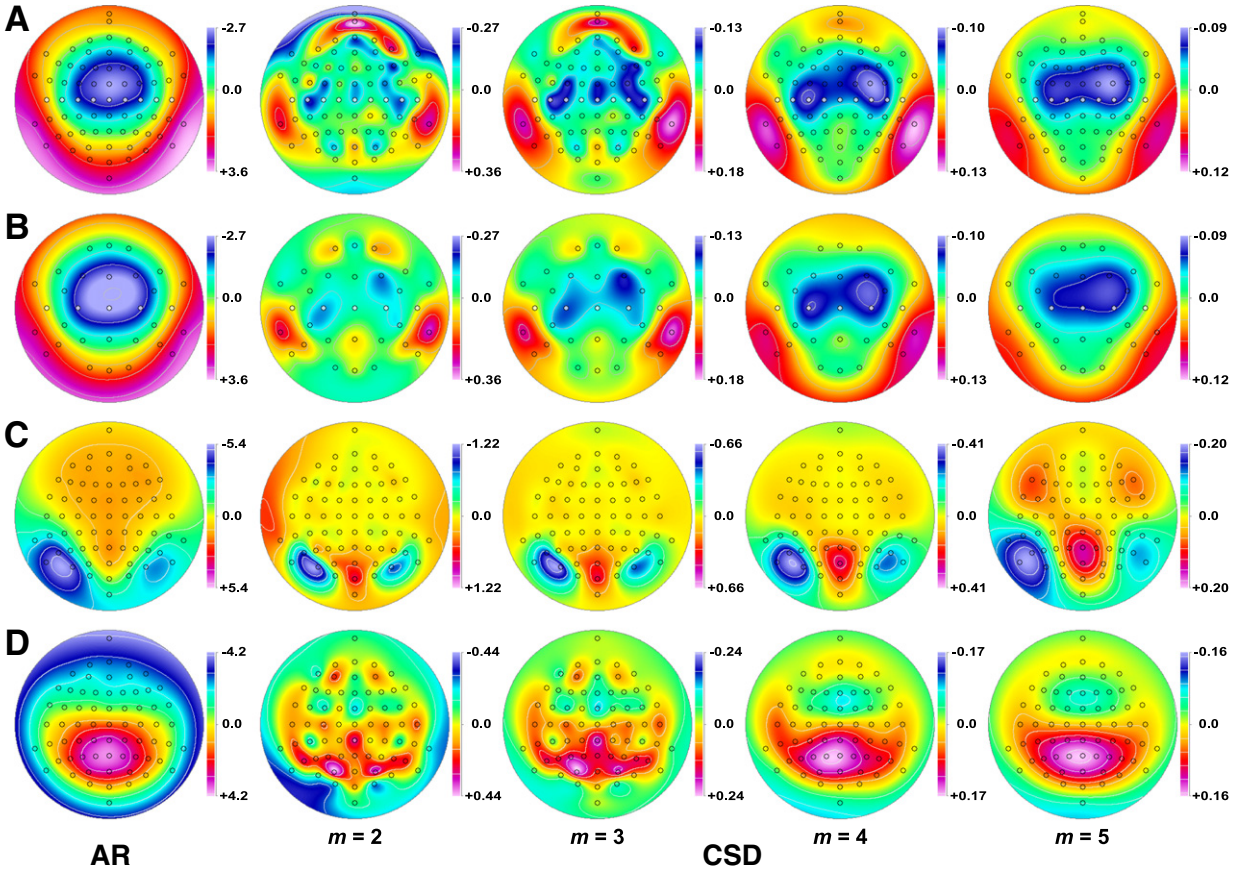

Fig. 8. A, B. Grand mean ERP [μV] topography of auditory N1 (AR: average reference; unpublished data, $N = 164$, 112 ms peak amplitude, 80 dB tones presented during a loudness intensity paradigm) and corresponding surface Laplacian estimates (CSD: current source density [μV/cm2]) using spherical splines of different flexibility ($m = 2$–5; $\lambda = 10^{-5}$; Perrin et al., 1989). Topographies were created for the original 72-channel EEG montage (A) and a subset consisting of 31 scalp locations (B). Gray circles mark scalp locations in the coronal plane. Due to the large differences in amplitude range associated with variations of spline flexibility, asymmetric scales were used to optimally represent the scalp distributions of ERP and CSD values; however, the ratios between positive and negative extremes are the same for each scale to preclude distortion of their relative value (i.e., green represents zero in all scales). C, D. Visual N1 and P3 (AR as shown in Fig. 2A) and corresponding CSD topographies of different spline flexibility ($m = 2$–5; $\lambda = 10^{-5}$) using symmetric scales adjusted to the data range for each map.

Finding an optimal regularization constant is of critical relevance for realistic Laplacian computation, and various regularization techniques have been proposed for this purpose (e.g., Bortel and Sovka, 2007, 2013). An optimal value for λ may be derived from the actual data by computing a cross-validation (CV) criterion that minimizes the prediction error for estimated potentials (i.e., using spherical spline interpolation to predict the data at any given site from the data of all other sites; e.g., Pascual-Marqui et al., 1988; Stone, 1974). Fig. 9 compares λ-optimized CSD topographies for an auditory N1, revealing that the spatial low-pass filter properties associated with less flexible splines (i.e., greater m constant) and more regularization or smoothing (i.e., greater λ value) can – to a certain degree – mutually compensate to achieve optimal potential estimates. As a consequence, λ-optimized CSDs obtained with different spline orders yield more similar surface Laplacian estimates (between-topography correlations were $0.6872 \le r \le 0.9970$) compared to those obtained with a fixed λ value (cf. Fig. 8A, which employed a default smoothing constant of $\lambda = 0.00001$ for all spline orders, yielding $0.3775 \le r \le 0.9693$ for 72 channels, and $0.6054 \le r \le 0.9714$ for 31 channels).

The estimation of an optimal regularization parameter from empirical data has an unfortunate byproduct: putative measures of interest, including different ERP components, EEG spectra or time-frequency measures, will be associated with different optimal λ values. This concern also applies to different experimental conditions, study groups, or individual subjects. Because it is rather undesirable to modify the spline computation algorithm within a given study or analysis, as a rule-of-thumb, previous 'optimal' λ values provide an appropriate choice, and eliminate the possibility of an arbitrary regularization parameter selection (cf. Nunez and Srinivasan, 2006). We have repeatedly found that a λ value of 10^{-5} serves as a robust regularization constant for a wide range of EEG/ERP applications for a commonly-used spherical spline order ($m = 4$), yielding surprisingly similar CV minima when compared with the CV optimum (e.g., for the N1 sink topographies shown in Fig. 9 with $m = 4$, optimal and default values of λ corresponded to CV criterion values of 9.4952 and 9.5264, respectively).

1.3.4. Spline iteration

The spherical spline interpolation of continuous surface potentials on the scalp surface, which is derived from the n discrete locations included in the EEG montage, involves a recurrence term to solve a Legendre differential equation of degree n (Perrin et al., 1989; cf. Eq. (3) in Kayser and Tenke, 2006a). To obtain a valid solution for this iterative series to yield a sufficient precision for creating a data transformation matrix, a minimum number of iterations are required. In general, a larger number of iterations will generate better results, however, as any improvements will become increasingly smaller with additional iterations, the computational costs will eventually outweigh their gain. Using a 19-channel EEG montage, Perrin et al. (1989) noted that a minimum of 7 iterations were required for a spline order of $m = 4$ to obtain a precision of 10^{-6}. Because the precision level will be affected by the spline order and montage density, a minimum of 20 iterations, but preferably 50 or more, is a good choice. Importantly, the time-consuming

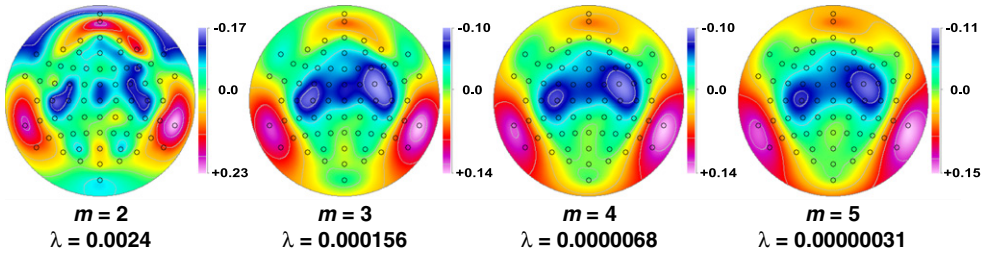

Fig. 9. Surface Laplacian estimates [μV/cm^2] employing optimized smoothing for different spherical spline orders ($m = 2$–5). The optimal value for λ was separately determined for each spline flexibility by computing the cross-validation (CV) criterion from the individual auditory N1 topographies ($N = 164$) at 112 ms constituting the overall grand mean 72-channel ERP topography (Fig. 8A). Accordingly, the sum of the squared differences between the observed potential and the estimated potential (i.e., using a 71-channel spherical spline interpolation with m flexibility and λ smoothing) was repeatedly computed for each of the 164 topographies at any site for different λ values to determine the minimum of the underlying function corresponding to a particular value of m (cf. Pascual-Marqui et al., 1988; Stone, 1974).

process for setting-up two montage-dependent transformation matrices (one for estimating the scalp distribution of surface potentials, and another one for the surface Laplacian), which will exponentially increase with montage density, must be done only once for a given montage. Once these two transformation matrices have been calculated, surface Laplacian estimates can be readily obtained for any sample point (i.e., any discrete EEG/ERP topography).[11]

2. Characteristic surface Laplacian topographies

The purpose of this section is to provide direct comparisons between surface potentials and surface Laplacian estimates for representative EEG measures in time and frequency domains, which are widely employed in the field and will therefore be familiar to most readers. Rather than reviewing specific findings reported in the literature, we aim to make the surface Laplacian transformation more transparent and less obscure using data recorded in our lab as convenient examples, with a focus on characteristic similarities and discrepancies in scalp distribution between surface potentials and the surface Laplacian. In this vein, we will not discuss any functional properties of these various measures, explicitly recognizing that any given measure may be employed in different cognitive paradigms, intended to serve different clinical objectives and research goals, and may be subject to interpretational discrepancies, all of which is beyond the scope of this paper. However, we note that surface Laplacian methods are ideally suited to help resolving existing controversies (e.g., Burle et al., 2015; Vidal et al., 2015).

2.1. Theta and alpha power

Quantitative EEG methods represent a cornerstone of basic and clinical research, effectively shaping a broad, diversified research agenda that addresses questions pertaining to anterior alpha asymmetries (e.g., Coan and Allen, 2004; Davidson, 1998), default mode network activation (e.g., Chen et al., 2008; Scheeringa et al., 2008), oscillatory band power and connectivity (e.g., Stam and van Straaten, 2012), working memory (e.g., Hsieh and Ranganath, 2014; Klimesch, 1999; Roux and Uhlhaas, 2014; Sauseng et al., 2005), or clinical treatment outcome (e.g., Pizzagalli et al., 2001; Tenke et al., 2011), to name just a few. A valid and reliable separation of EEG spectra is of critical importance for all of these questions, particularly if the primary interest concerns neighboring frequency bands, such as theta (4–8 Hz) and alpha (8–13 Hz). Fig. 10 shows EEG amplitude spectra for a single individual performing an auditory working memory paradigm, which requires identifying the correct position of a probe letter within an initial letter series. While performing this task for trials spanning several seconds, both frontal midline theta and parietal alpha oscillations, which may subserve crucial functions of memory and cognition, constitute the dominant frequencies regardless of EEG reference or surface Laplacian transformation. However, the topographic maxima for theta at AFz and alpha at POz are largest for CSD-transformed spectra (Fig. 10A), resulting in focused CSD scalp distributions (Fig. 10B, C). In contrast, surface potential spectra render a less sharp, more distributed topography, which may include substantial spectral amplitudes at other sites (e.g., nose-referenced theta in Fig. 10B). For better comparison, EEG spectra were also plotted for nearby locations (i.e., at F3 for theta and at P3 for alpha). At these off-maximum sites, the smallest spectral amplitudes are seen for CSD estimates. Moreover, a small alpha peak can be observed at F3, which is most distinct for the average reference. It is also not a coincidence that low or zero spectral amplitudes (dark blue regions in Fig. 10B, C) can be seen over anterior regions (Nose, Nz) for the nose-referenced data but over lateral inferior temporal-parietal sites (TP9/10, P9/10) for the linked-mastoids reference, and zero amplitudes are suspiciously absent for the average reference. These spurious effects, which can be attributed to volume conduction, reference location and arithmetic (i.e., computation of an average reference), are considerably diminished by the surface Laplacian.

Another important notion concerns the different topographies across reference schemes. In contrast to ERP topographies, which do not change after converting to a different reference (i.e., the between-topography correlations depicted in Fig. 6A for either N1 or P3 are all $r = 1.0$), spectral topographies differ substantially between EEG references (for theta, $0.0548 \le r \le 0.3707$; for alpha, $0.6895 \le r \le 0.8697$), because spectral estimates are derived from nonlinear data transformations (cf. Fig. 1 in Tenke and Kayser, 2005). Thus, topographies of spectra and, by extension, of all oscillation measures based on power spectra, including phase locking, coherence, event-related spectral perturbations and many more, are affected by the choice of reference – CSD-based spectral measures are not (e.g., cf. Fein et al., 1988; Guevara et al., 2005; Schiff, 2005).

2.2. P3a and P3b

The classical P3(00) is probably the most studied ERP component (e.g., Donchin, 1981; Donchin and Coles, 1988; Nieuwenhuis et al., 2005; Verleger, 1997), not least because of its omnipresence across ERP paradigms and study groups (although to a different degree) and

[11] Although the surface Laplacian has been implemented in various commercial software packages and free academic tools, the particular algorithm used is not always made explicit. Moreover, user-friendliness, data compatibility and availability to export the CSD-transformed data differ greatly, and critical algorithm parameters (spline flexibility, regularization and iteration constants) may use default values and may therefore not be under user control. Kayser and Tenke (2006a, Appendix) published a Matlab implementation for spherical spline CSD estimates proposed by Perrin et al. (1989), which was later expanded to the freely-available *CSD Toolbox* (Kayser, 2009) that provides a convenient means to exercise control over all essential aspects of a spherical spline SL transform.

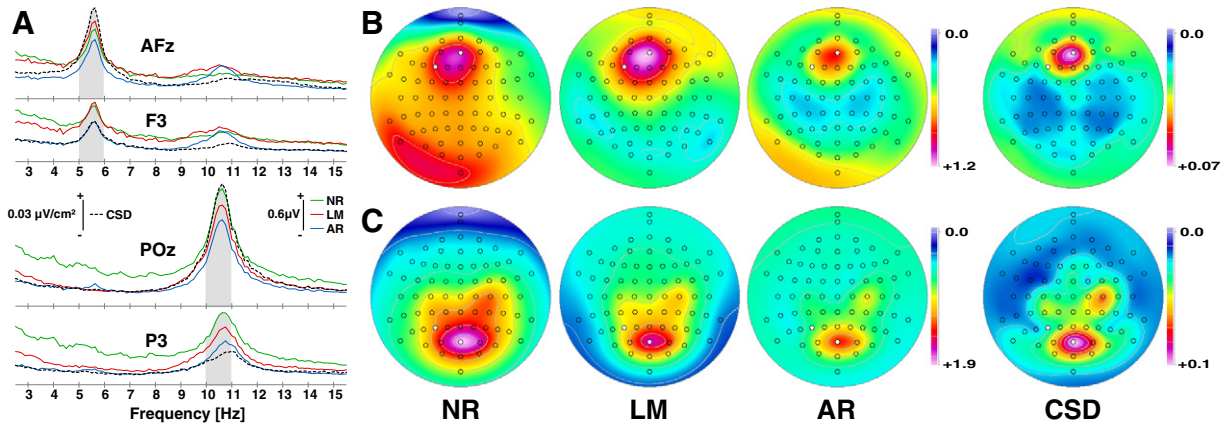

Fig. 10. Frequency spectra (3–15 Hz) at selected anterior (AFz, F3) and posterior (POz, P3) sites (A) and corresponding peak theta (5–6 Hz) and peak alpha (10–11 Hz) scalp distributions (B, C; mean of shaded frequency ranges in A) of an individual participant during an auditory working memory task. Shown are mean fast Fourier transform (FFT) amplitudes derived from 220 8-s epochs (72-channel EEG montage, 256 samples/s, 20% Hanning taper window, resolution 0.125 Hz) converted to common surface potential [µV] references (NR: nose reference; LM: link-mastoids reference; AR: average reference) and also transformed to current source densities (CSD [µV/cm^2]; spherical spline parameters: $m = 4$, $\lambda = 10^{-5}$, 50 iterations; Perrin et al., 1989). Anterior and posterior sites were selected to reflect both the topographical maximum of theta and alpha as well as nearby (off-maximum) locations (marked circles in B and C).

its resilience to masking by common reference choices, all of which may have contributed to its early discovery (Sutton et al., 1965). Its hallmark characteristic is a mid-parietal maximum, but other ERP positivities with similar peak latencies and different topographies have since between identified, together forming a family of ERP components often referred to as the *late positive complex* (Sutton and Ruchkin, 1984). Two subcomponents, termed P3a and P3b, have generated a considerable amount of research interest: P3b, which is synonymous to the classical P300, is hypothesized to reflect effortful allocation of attention and subsequent memory processing, while P3a, which peaks earlier than P3b and has a relatively more frontal midline maximum, is assumed to reflect stimulus-driven attentional processes (e.g., reviewed by Polich, 2007). Because of their temporal and spatial overlap, it may be difficult to disentangle these two components unless appropriate experimental manipulations are employed; however, multivariate analytic approaches have also been proposed to accomplish an adequate separation (e.g., Spencer et al., 1999, 2001).

An often employed paradigm that reliably generates both P3a and P3b is the so-called novelty oddball paradigm (e.g., Fabiani and Friedman, 1995), a modified 3-stimulus version of a classic 2- stimulus target detection task. Participants are instructed to respond to infrequent tones (targets, 10% probability) embedded in a series of frequent tones of different pitch (nontargets, 80%) as well as infrequent stimuli consisting of unique environmental sounds (novels, 10%), which are to be ignored. In this paradigm, a P3b is mostly observed for targets, whereas a P3a is primarily seen for novels (and hence also called novelty P3). Fig. 11 shows target and novel ERPs at midline sites Cz and Pz, which were recorded from 49 healthy adults during this novelty oddball task (for details, see Tenke et al., 2010). As noted above, P3b amplitudes and latencies at Pz for targets varied markedly between EEG references, showing larger and earlier peaks for ERPs referenced to linked mastoids or nose (peak latencies 340 ms and 350 ms) compared to the common average (370 ms; Fig. 11A), notwithstanding the fact that their window-based P3b topographies having a broad mid-parietal maximum were identical (i.e., their between-topography correlations are all $r = 1.0$; Fig. 11D, left columns). The corresponding CSD waveforms also had a positive maximum at Pz (375 ms), but revealed a more refined parietal P3b distribution with sources extending anteriorly along temporal regions but sparing central sites (Fig. 11D, right column).

Likewise, P3a amplitudes and latencies at Cz for novels also differed between EEG references, peaking somewhat earlier for ERPs referenced to nose or linked mastoids (320 ms and 325 ms) compared to P3b, but considerably earlier for the average reference (260 ms; Fig. 11B). Still, a notable deflection can also be seen at this latency in the nose- and linked-mastoids ERPs. Again, all P3a ERP topographies show an identical broad scalp distribution with a vertex maximum (Fig. 11E, left columns). In sharp contrast, the corresponding CSD waveforms had a distinct positive maximum at Cz (255 ms), with sources extending laterally and posteriorly along mid-parietal sites (Fig. 11E, right column). Considering the time course (i.e., early and late P3 intervals) of both conditions (target, novel) together, the surface Laplacian estimates reveal two distinct positive components having separate scalp distributions (Fig. 11C–F, right column). The CSD equivalent of the P3a, termed novelty vertex source (NVS) on the basis of its functional and topographic properties, is a reliable phenomenon across different healthy and psychiatric populations (Kayser et al., 2014; Tenke et al., 2010). Obviously, no such clear distinction between P3a and P3b can be made on the basis of surface potentials.

2.3. Mismatch negativity (MMN)

Auditory MMN, a pre-attentive measure of auditory change detection, enjoys almost the same popularity as the P3, as it can be easily studied in a wide range of healthy and clinical populations (e.g., for reviews, see Michie, 2001; Näätänen, 1990; Näätänen and Picton, 1987; Näätänen et al., 2012). Although the advantages of CSD transformations of MMN ERPs have recently been highlighted by Giard et al. (2014), MMN provides a convenient example for a prototypical ERP component derived from difference waveforms. The MMN paradigm effectively constitutes a passive oddball task, in which infrequent events (deviants) are embedded in a series of frequent events (standards) but subjects are not required to respond to the infrequent events, which typically differ from the frequent events in one or more physical stimulus property (e.g., frequency, duration, intensity). Rather, the subject's attention is commonly directed towards a different task (e.g., reading a book or watching a movie), which also influences the MMN (e.g., Müller-Gass et al., 2005). The MMN itself is a prominent 'negative' deflection in the ERP difference waveforms of deviants and standards (i.e., the component's polarity is determined by convention), peaking approximately around 150 ms, but notably after the N1 peak, and showing a broad frontocentral maximum. However, by employing a surface Laplacian for MMN data obtained during a directed attention (dichotic listing) task, Giard et al. (1990) found strong topographical evidence for two distinct MMN components comprising frontal and temporal neural generators, which could not be distinguished in the surface potentials.

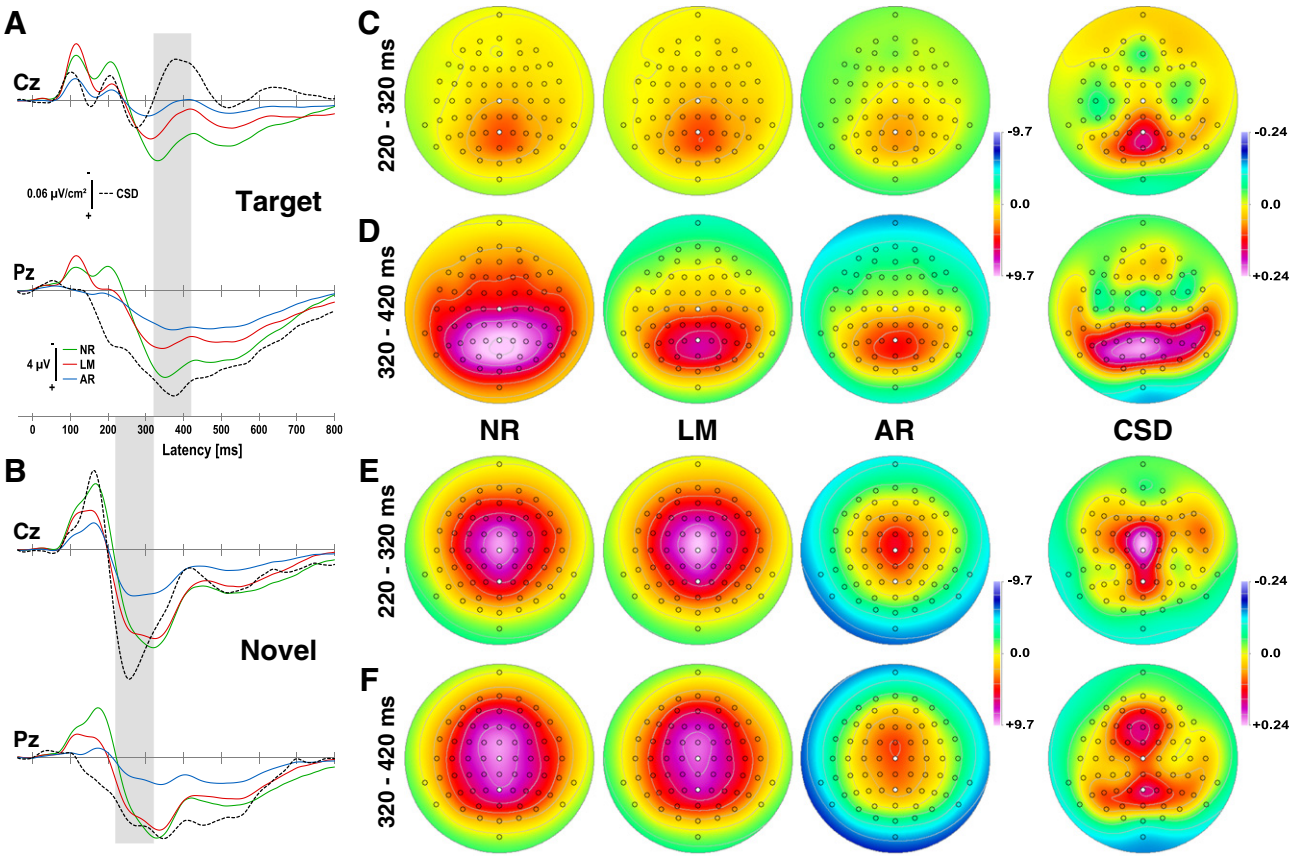

Fig. 11. Grand mean waveforms (−60 to 800 ms) at selected midline sites (Cz, Pz) for target (A) and novel (B) stimuli and corresponding topographies of mean P3b (time interval 320–420 ms) and P3a (220–320 ms) amplitudes (C-F; shaded ranges in A and B) recorded during an auditory novelty oddball task (data of 49 healthy adults from Tenke et al., 2010). Compared are common surface potential [μV] references (NR: nose reference; LM: link-mastoids reference; AR: average reference) and the surface Laplacian transformations (CSD [μV/cm^2]; spherical spline parameters: $m = 4$, $\lambda = 10^{-5}$, 50 iterations; Perrin et al., 1989). Selected intervals and sites correspond to latency peaks and topographical maxima of P3b and P3a (marked circles in C–F).

The MMN depicted in Fig. 12 was measured during a tone series consisting of repetitive standards that were infrequently interrupted by pitch deviants (80%:20% probability; 300 ms duration; 600 ms SOA). Standard tones (either 485, 680, 953 or 1336 Hz) were combined with deviant tones constructed to reflect easy (.67, .75) or difficult (.90, .95) discrimination ratios to create 8 120-trial blocks. Each block consisted of one standard tone and 4 deviant tones (5% each with a lower or higher frequency at each ratio), which were arranged in a pseudo-randomized sequence. During these 8 blocks (960 trials), ERPs were recorded from 8 healthy adults, who were instructed to watch silent movie clips (wildlife scenes) and ignore the tones. For the present purpose, all deviants were pooled and MMN was computed from deviant-minus-standard difference waveforms.

MMN amplitudes and latencies again varied between EEG references at different sites, showing the largest mid-frontocentral MMN for ERPs referenced to linked mastoids (peak latency 150 ms at Cz) and the

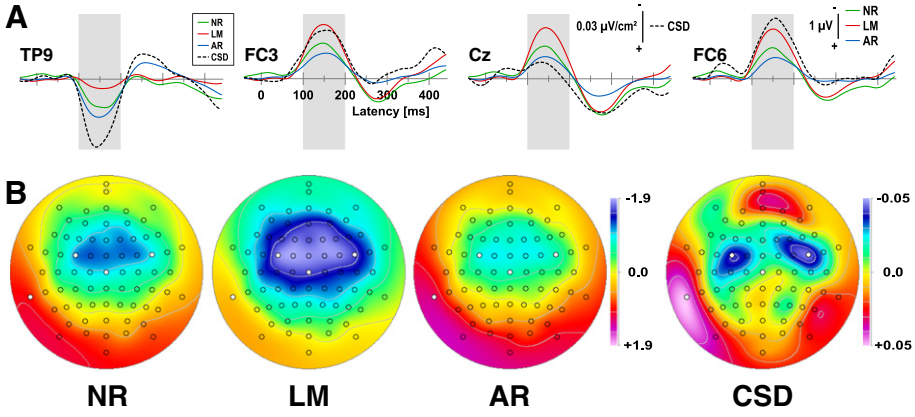

Fig. 12. Grand mean difference waveforms (−40 to 440 ms) at selected sites (TP9, FC3, Cz, FC6) derived from deviant-minus-standard tones (A) and corresponding mismatch negativity (MMN) topographies (B; mean amplitudes for time interval 100–200 ms as indicated by shaded ranges in A) recorded during a frequency (pitch) MMN paradigm (unpublished data of 8 healthy adults, 72-channel EEG montage, 256 samples/s; see text for further method details). Selected sites correspond to topographical MMN minima and maxima (marked circles in B), which differ between ERP and CSD data (ERP references and CSD transformations as in Fig. 11).

smallest MMN for the average reference (160 ms; Fig. 12A). At the same time, MMN inversion at lateral-inferior temporoparietal sites (cf. TP9) was largest for the average reference and smallest for the linked-mastoids reference, as it should be because these ERP difference topographies are not affected by the EEG reference choice (i.e., for all between-topography correlations, $r = 1.0$). In contrast to the surface potential MMN topography, its CSD counterpart revealed off-midline (i.e., bihemispheric) frontocentral MMN maxima corresponding to temporoparietal MMN minima, similar to the auditory N1 CSD topography depicted in Figs. 8 and 9. Indeed, despite profound differences in amplitude and latency, the topographies of N1 (for LM at Cz: peak latency 125 ms, peak amplitude 3.1 μV) and MMN and were almost identical for this sample ($N = 8$; for ERP, $r = 0.9854$; for CSD, $r = 0.9480$), suggesting that the same neuronal tissue (i.e., primary auditory cortex) contributed to the generation of both N1 and MMN (cf. May and Tiitinen, 2010).

2.4. Response-related midfrontal negativities

Since the discovery of a negative response-locked ERP component prompted by incorrect choice reactions, then termed the error negativity (Ne) or error-related negativity (ERN; e.g. Falkenstein et al., 2000; Gehring et al., 1993), there has been a growing interest in medial frontal negativities associated with performance monitoring involving activation of the anterior cingulate cortex (e.g., for reviews, Hoffmann and Falkenstein, 2012; van Veen and Carter, 2002; van Noordt and Segalowitz, 2012). An ERN-like component can also be observed in the absence of an erroneous response, that is, for correct choices; however, this correct response negativity (CRN/Nc) is substantially smaller and largely masked in surface potentials, and was only discovered by use of the surface Laplacian (Vidal et al., 2000). Notably, a CRN can also be observed in stimulus-locked CSD waveforms recorded during a typical oddball paradigm (Kayser and Tenke, 2006a).

This phenomenon – CRN presence in SL waveforms but virtual absence in their ERP counterparts – is shown in Fig. 13 for 129-channel EEGs recorded from 17 healthy adults during an oddball paradigm with complex tones or consonant-vowel as stimuli (Kayser and Tenke, 2006b). In different task blocks, participants were instructed to respond to targets (20% probability) with a left or right button press (for further details, see Kayser and Tenke, 2006a). Data were pooled across tonal and phonetic stimuli and included about 50 trials for each response hand ($M \pm SD$: for left press, 49.6 ± 7.0, range 39–61; for right press, 47.8 ± 9.7, range 24–63). The response-locked CSDs reveal a distinct mid-frontocentral negativity (sink) that is restricted to the right hemisphere (cf. electrode location 107, which is approximately site FCC2h in the 10–5 system; Jurcak et al., 2007) for left hand responses, and to the left hemisphere (cf. location 13, approximately FC1) for right hand responses (Fig. 13A, column 2 and 3; Fig. 13B, column 4). These unilateral midfrontal sinks are accompanied by bilateral centroparietal sources, which are also more distinct over the hemisphere contralateral to the response hand (cf. location 94, approximate CCP4, for left press; location 43, approximate CCP3, for right press). In contrast, the response-locked ERPs reveal almost no midfrontal negativity, although minor deflections are detectable for linked-mastoids and average references at locations 107 and 13. Much of the response-locked ERP scalp topography is characterized by a broad positivity resembling a parietal P3b, particularly for the nose reference because the most negative potential is at the nose. Still, asymmetric shifts can nevertheless be deduced in this topography from the isopotential lines, which are consistent with a frontal negativity contralateral to the response (again, the topographies for each response hand do not differ between references).

The stimulus-locked CSDs reveal a highly similar sink-source topography during a time interval (420–580 ms; Fig. 13D, column 4) following the mean response latency ($M \pm SD$: for left press, 426 ± 89 ms; for right press, 464 ± 95 ms), projecting the CRN peak latency within the range of 480 to 520 ms post stimulus onset. At a frontocentral midline site (location 6, approximately FFCz), a robust sink activity is observed in the CSD waveforms (Fig. 13C, column 2); no negativity is seen in the ERPs, which nevertheless expose suspicious deflections during this period, although these occur during the receding slope of the P3b peaking around 350 ms. While this P3b maximum is observed at mid-parietal sites for stimulus-locked ERPs and CSD alike (cf. location 62, approximately CPPz; Fig. 13C, column 3), only the CSDs reveal a distinct bilateral centroparietal source (cf. locations 38 and 88, approximately CCP3h and CCP4h; Fig. 13C, column 1 and 4; Fig. 13D, column 4) during the later, response-related interval. This stimulus-locked mid-frontal sink and centroparietal source pattern is entirely different from a P3b source topography (cf. Fig. 11D, right column), but highly similar to the response-locked ERN-like CSD topography. This mid-frontal, response-related negativity (FRN) can be reliably observed in stimulus-locked CSD waveforms during different cognitive paradigms and study populations employing less-dense EEG montages (Kayser and Tenke, 2006a, 2006b; Kayser et al., 2007, 2009, 2014; Tenke et al., 2008, 2010); however, it remains largely hidden in stimulus-locked ERPs.

3. Common surface Laplacian concerns

Despite awareness of the theoretical advantages afforded by the surface Laplacian, first and foremost its independence of the EEG recording reference and ability to enhance the spatial information of the EEG signal (i.e., 'high-resolution EEG'; Gevins et al., 1995; Nunez and Pilgreen, 1991; Nunez and Westdorp, 1994; Nunez et al., 1994), persistent reservations throughout the field have prevented a widespread and systematic use of these methods. Paradoxically, less straightforward data transformations, including multivariate data decomposition techniques and inverse solutions, which typically involve biophysical assumptions about tissue conductivity and geometry or number, orientation and independence of neuronal generators, have by far enjoyed a higher level of popularity among EEG researchers. This section directly addresses the validity and implications of these objections from a pragmatic perspective, focusing on the SP versus SL comparison.

3.1. Surface potentials have a proven history

Clinical and basic EEG research relish a remarkable, almost century long, history of scientific success that has generated a vast number of breakthrough findings in many areas using surface potentials. Although the overwhelming majority of electrophysiologists appears to be cognizant of the reference problem, the direct implications of this dependency for EEG data analysis have been underestimated or dismissed. It is generally presumed that simply by applying the *same* EEG reference (e.g., average or linked-mastoids), whatever its specific problems or

Fig. 13. Response- (A) and stimulus-locked (C) grand mean waveforms ($N = 17$) recorded with a 129-channel geodesic sensor net EEG system (Tucker, 1993) during tonal and phonetic oddball tasks requiring a left or right response button press to target stimuli (data from Kayser and Tenke, 2006b). Baseline corrections for response- and stimulus-locked ERPs are −300 to −100 ms and −100 to 0 ms, respectively. Topographies correspond to a mid-frontal response-related negativity (FRN) peaking at about 50 ms post response (B: mean amplitude during time interval 25–75 ms; shaded ranges in A) and approximately 500 ms post stimulus onset (D: 420–580 ms; shaded ranges in C). Selected sites (see insets for electrode names in A and C) were left mid-central (43), left frontocentral (13), right frontocentral (107) and right mid-central (94) for response-locked waveforms, and left and right central (38, 88), mid-frontocentral (6) and mid-centroparietal (62) for stimulus-locked waveforms, which approximated CSD sink and source maxima (marked circles in B and D; ERP references and CSD transformations as in Fig. 11).

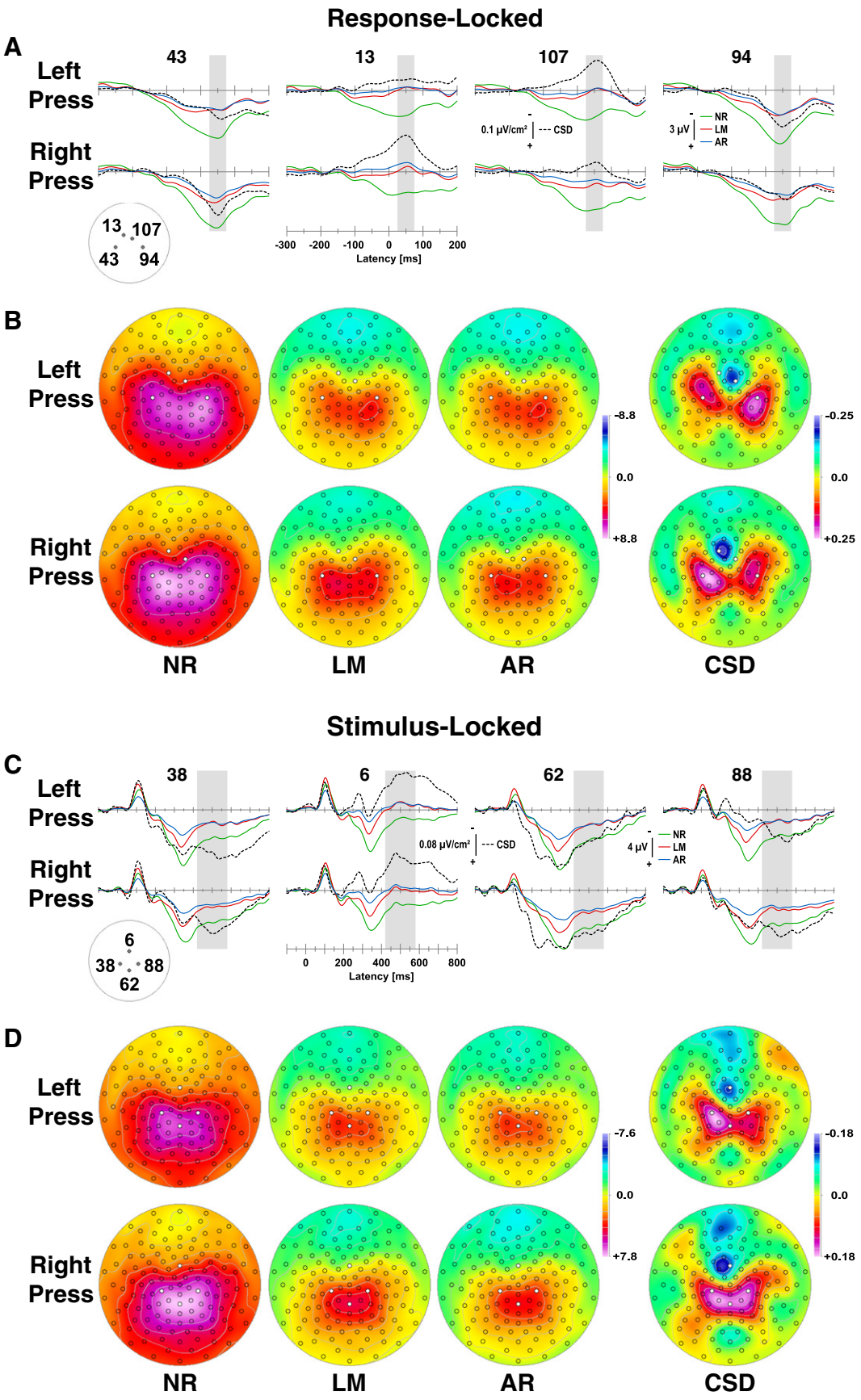
Response-Locked
A
Left Press
Right Press
43
13
107
94
0.1 µV/cm²
CSD
3 µV
NR
LM
AR
-300 -200 -100 0 100 200
Latency [ms]
B
Left Press
Right Press
-8.8
0.0
+8.8
-0.25
0.0
+0.25
NR
LM
AR
CSD
Stimulus-Locked
C
Left Press
Right Press
38
6
62
88
0.08 µV/cm²
CSD
4 µV
NR
LM
AR
0 200 400 600 800
Latency [ms]
D
Left Press
Right Press
-7.6
0.0
+7.8
-0.18
0.0
+0.18
NR
LM
AR
CSD

disadvantages, the data at hand are treated equally and all group- and/or condition-differences can be attributed to the experimental manipulation, which, if smartly designed, will warrant factual and accurate interpretation of findings. However, these presumptions are deceiving, as exemplified by Figs. 2 and 3 and generalized by the schematics shown in Fig. 14.

Let us assume that a certain process or function (i.e., condition, group, or interaction thereof) is represented by neuronal generator activity that may be conceptually summarized by a single dipole, and that a second process is represented by a different neuronal activation resulting in a dipole of the same strength but with a different orientation (Fig. 14A). If the surface potentials stemming from either dipole are recorded from two scalp sites, one serving as the reference for the other, placed in line with the orientation of one the two dipoles, a greater potential will be measured for the in-line dipole (green) compared to the out-of-line dipole (red). This will lead to the conclusion that the first process (green) yielded a larger EEG signal than the second process (red). In contrast, if the surface potentials stemming from the same two dipoles are measured from two scalp sites placed at a right angle to the orientation of the green dipole (Fig. 14B), a greater potential will be measured for the red dipole. Hence, this reference scheme will lead to the opposite conclusion (i.e., the second process yielded a larger EEG signal than the first process). Even if the two processes are represented by the same dipole (same orientation), although to a different degree, the choice of EEG reference will influence the measured SP amplitudes. Whereas the in-line reference arrangement will render a green-larger-than-red result (Fig. 14C), the orthogonal reference arrangement will reveal no differences (zero amplitudes) between the two processes (Fig. 14D). These unfortunate ambiguities apply to *all* surface potential measures in time, frequency and time-frequency domains, however, becoming increasingly more convoluted with multiple neuronal generators overlapping in space and time and greater complexity of the EEG measure. Without doubt, many misconceptions and controversies in EEG and ERP research have their root in the use of difference reference schemes (e.g., Joyce and Rossion, 2005).

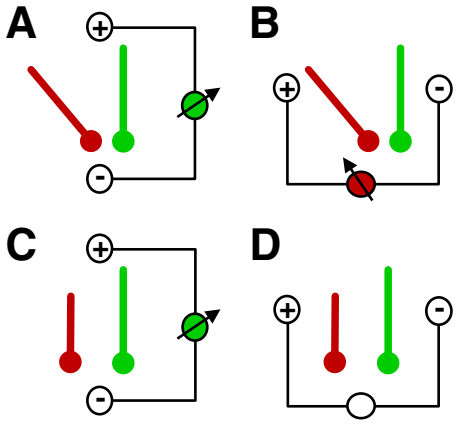

Fig. 14. Schematic of interaction between the strength and orientation of a neuronal generator (modeled as a dipole) and choice of EEG reference. Assumed are two hypothetical EEG reference schemes in which reference (−) and recording (+) sites are either placed in line (A, C) or perpendicular (B, D) to the orientation of one dipole (green). A. Two dipoles of equal strength but different orientation will yield different surface potentials in favor of the green dipole which orientation best matches the alignment of reference and recording site. B. The same constellation of dipoles will favor the red dipole if reference and recording site are vertically aligned to the green dipole (i.e., rendering no potential difference between reference and recording site). C. Two dipoles of different strength but equal orientation will favor the green dipole if reference and recording site are aligned in parallel to the orientation of these dipoles. D. However, even in this scenario, a vertical alignment of reference and recording site to the orientation of these dipoles will render the same (i.e., zero) surface potential for either dipole.

Even if the declared research goal is the understanding of psychological functions and not the delineation of the underlying functional neuroanatomy, the fact that brain activation is responsible for the EEG phenomena used to study psychological functions and because the measured outcome can be reversed by changing the reference should be enough reason for concern. While there may be an optimal EEG reference for a given constellation of neuronal generators (e.g., Fig. 14C; cf. also Dien, 1998), the neuronal generators under study are typically not known in advance and consist of more than a single dipole. Thus, from a purely pragmatic perspective, the use of an ambiguous activation measure seems highly undesirable, and should be replaced with a non-ambiguous measure as long as this alternative will not introduce considerable costs offsetting these benefits.

3.2. Loss of signal with low spatial frequency

Among the strongest arguments against the (exclusive) use of the surface Laplacian is the notion that EEG signals of low spatial frequency (i.e., originating from deep and/or distributed generator sources) are suppressed by a spatial high-pass filter (e.g., Nunez et al., 1997, 1999). For simulated radial and tangential dipoles, Perrin et al. (1987) plotted the different attenuation (fall-off) of CSDs and field potentials as a function of generator distance d (eccentricity) from the scalp surface. This attenuation is sharper for CSDs ($1/d^3$ versus $1/d$), indicating that the surface Laplacian emphasizes shallow, cortical generators. However, in this recently reproduced plot (Giard et al., 2014), both attenuation curves were adjusted by their respective peak maxima, ergo allowing no conclusions about how well (or reliable) each measure represents or "sees" brain activity of any given deep or shallow generator (i.e., without a direct, cross-measure comparison). Stated differently, this comparison between SP and SL measures implicitly assumes that 1) both measures are equally good in reflecting the signal maximum, and 2) larger values (or values per se) reflect a signal.

In their landmark textbook, Nunez and Srinivasan (2006) have stressed that compared to surface potentials, spatial band-pass filtering of distributed cortical sources reduces surface Laplacian estimates of large dipole layers in favor of smaller dipole layers. Forward simulations with a four-shell head model as a function of radial dipole layer size and different ratios of brain-to-skull conductivity revealed the maximum scalp potential for broad dipole layers (extending about 7–10 cm), whereas the surface Laplacian maximum was observed for small dipole layers (about 2.5 cm; cf. Fig. 8–7 on p. 328 in Nunez and Srinivasan, 2006). However, these simulations were based on three-dimensional spline interpolations (Nunez and Srinivasan, 2006, Appendix J), which closely correspond to surface Laplacian estimates based on highly flexible spherical splines ($m = 2$–3; e.g., Perrin et al., 1989).

Fig. 15 shows these relations between cortical dipole layer size and EEG surface measures for two different brain-to-skull conductivity ratios. Scalp potentials were simulated for a fully-balanced, 81-channel 10–10 system EEG montage (Oostenveld and Praamstra, 2001) using a four-shell forward solution (Berg, 2006) with radial dipoles located 14 mm below the outer scalp surface (85 mm head radius), expanding in 'cap size' from a focal dipole underlying Cz (0 cm) to a broad circle of 135° downward in steps of 3° (20 cm). Corresponding CSD estimates were calculated from these surface potentials using spherical spline interpolations with different flexibility constants ($m = 2$–7; $\lambda = 10^{-5}$; Perrin et al., 1989). These simulations replicate those reported by Nunez and Srinivasan (2006) for both surface potentials (maxima at about 8–9 cm; Fig. 15A and B) and surface Laplacian estimates when using a high spline flexibility (i.e., $m = 2$ or $m = 3$; maxima at about 2.5-3 cm; red and green lines in Fig. 15C and D). They also confirm that the relative magnitudes of different spatial frequencies (i.e., the surface Laplacian transform acts as a spatial filter) are not affected by different brain-to-skull conductivity ratios. Most importantly, however, surface Laplacian estimates based on more rigid splines become gradually more sensitive to broader dipole layers (approximate maxima for

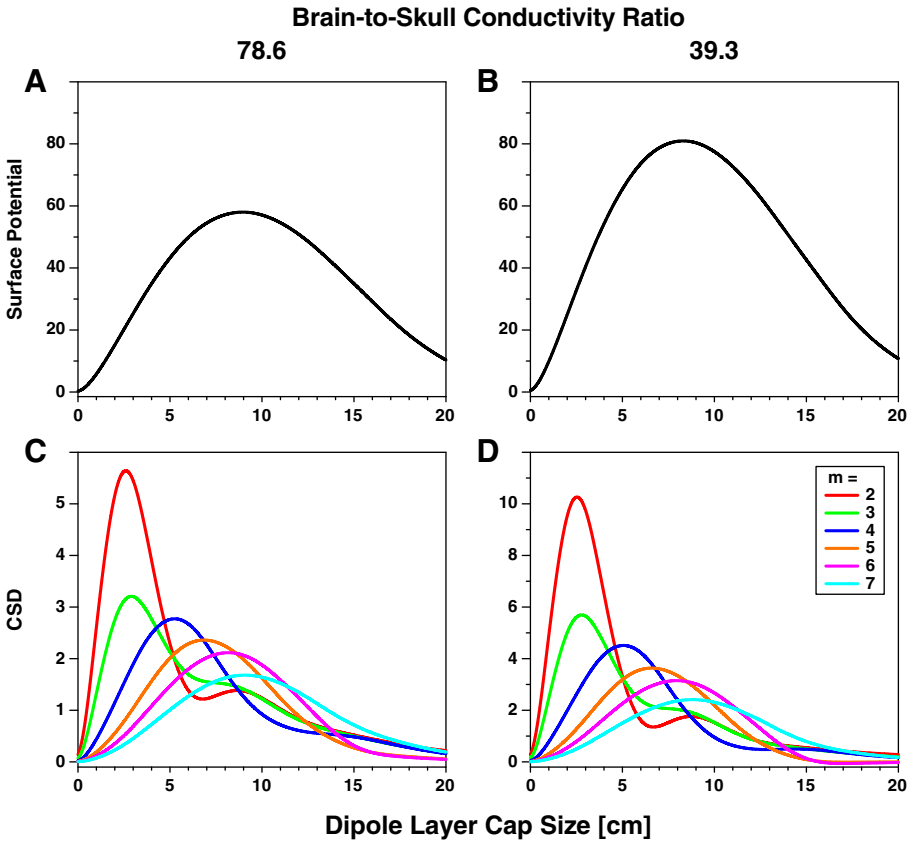

Fig. 15. Ratio of scalp measure to cortical potential as a function of dipole layer size. A, B: Vertex scalp potentials for a 81-channel 10–10 system EEG montage (average reference) due to simulated dipole layers of varying angular extent, forming superficial spherical caps in a four-shell forward solution (Berg, 2006) for two different ratios of brain-to-skull conductivity with the following conductivities [S/m]: brain = 0.33, skull = 0.0042 (A: ratio = 78.6) or 0.0084 (B: ratio = 39.3), CSF = 1.0, scalp = 0.33. C, D: Corresponding surface Laplacian estimates (CSD: current source density) using spherical splines of different flexibility ($m = 2$–7; $\lambda = 10^{-5}$; Perrin et al., 1989). Note that surface potentials are primarily sensitive to broad dipole layers, whereas the sensitivity of spherical spline surface Laplacian estimates varies with spline flexibility.

$m = 4$–7 were 5, 7, 8 and 9 cm, respectively; Fig. 15C and D). Thus, the sensitivity of spherical spline SL estimates varies with the spline flexibility constant, with $m = 7$ closely corresponding to the spatial scale of surface potentials, and these relations are also not affected by different brain-to-skull conductivity ratios.

Nunez and Srinivasan (2006, 2014) have repeatedly emphasized that scalp EEG measures exhibit distinct dynamics at different spatial scales, concluding that unprocessed surface potentials and SL estimates (high resolution EEG) provide complementary information about neocortical dynamics. Whereas ERP components are rather confined in spatial scale, with P3b probably revealing the broadest scalp distribution, synchronized oscillations may be present on a larger spatial scale, involving rhythmic activations of anterior and posterior regions, which will be suppressed (i.e., spatially filtered) by SL estimates based on flexible splines (Nunez and Srinivasan, 2014). For example, Srinivasan (1999) reported that the spatial structure of alpha rhythm coherence differs between adults and children due to the endogenesis of maturing brain tissue, with overall large-scale (>20 cm) cortical dynamics in adults insufficiently represented by flexible spline SL estimates.

Consequently, functional connectivity and coherence measures based on SL estimates that only represent a smaller spatial scale (i.e., less than 5 cm) will not be able to detect these long-range oscillations. However, simulations of broadly-distributed sine and cosine generator sources indicated superior representations of amplitude and phase for CSD measures compared to surface potentials (nose, linked-mastoids, or average reference) when using a less flexible spline constant ($m = 5$; Tenke and Kayser, 2015a). It will be important to further investigate whether SL estimates based on less flexible splines, which can be adjusted to match the spatial scale of surface potentials (Fig. 15), are suited to overcome these limitations for different EEG applications. Importantly, coherence estimates are also subject to adverse effects of volume conduction and the recording reference (e.g., Fein et al., 1988; Guevara et al., 2005), particularly for EEG montages affording insufficient scalp coverage (i.e., 32 or fewer channels; e.g., Marzetti et al., 2007), which are still common in clinical settings as well as basic research.

Ultimately, the crucial question is to what degree surface potentials or Laplacian estimates can represent genuine brain activity. Using EEGs recorded from a large sample ($N = 130$) during a visual half-field paradigm, we found that CSDs revealed by far a more accurate representation of hemifield-dependent asymmetries of the posterior contralateral N1, both in time and time-frequency domains, than their surface potentials counterparts, regardless of reference scheme (average, nose, linked mastoids, reference electrode standardization technique [REST]; Kayser and Tenke, 2015). In contrast, surface potentials also revealed significant hemifield-dependent asymmetries at more anterior locations, which were presumably caused by volume conduction. Likewise, using forward simulations of sine and cosine waveforms originating from subdural and deep local generators, signal fidelity in topography and phase of the measured amplitude spectra was superior for CSD compared to surface potentials, even for deep generators (Tenke and Kayser, in 2015a). Moreover, posterior alpha rhythms observed at rest, during task performance or as event-related desynchronizations were consistently and appropriately represented by CSD measures when systematically compared to surface potentials (Tenke and Kayser, 2015b).

The considerations outlined in this tutorial review show that spatial high-pass properties of the surface Laplacian transform may be tailored to the research objective by the use of spherical splines with appropriate parametric choices for flexibility and regularization (cf. Figs. 8, 9 and 15). In fact, rigid splines and heavy regularization could be used to spatially low pass a topography that is virtually identical to a surface potential topography, however, it would still be reference-free. While this may appear to counter the advantage of the surface Laplacian, it would directly serve the need to maintain low spatial frequencies in the EEG signal, if this was an important concern (e.g., Nunez et al., 1999). Although this objective is incompatible with the maxim of minimizing surface Laplacian estimates with respect to the 'analytic' surface Laplacian distribution, which is better for more flexible splines (i.e., $m = 2$ or $m = 3$; Babiloni et al., 1995), the recommendation to use the surface Laplacian as a supplement to surface potential analysis implies an even greater discrepancy by prioritizing reference-dependent topographies without regard for the impact of volume conduction. Surface Laplacian estimates obtained with less flexible spherical splines operate on a spatial scale (i.e., intermediate for $m = 4$) that is not only suitable for low-density EEG recordings but also appears to be quite useful for high-density EEG (Kayser and Tenke, 2006b; Tenke and Kayser, 2012). Of course, less flexible splines come with the costs of giving up on sharpening EEG topographies, one of the embraced advantages of the surface Laplacian, but this impediment also applies to surface potentials.

3.3. Dense spatial sampling is a prerequisite

The quest for the most accurate estimation of the surface Laplacian has invigorated the prevalent understanding that a high spatial sampling of the EEG signal is necessary to avoid spatial aliasing and other topographic misrepresentations (e.g., Junghöfer et al., 1997; Nunez et al., 1994; Srinivasan et al., 1996, 1998b). However, this premise either dismisses the usefulness of low density EEG (i.e., less than 64 and more channels) outright, or it ignores the evidence that the surface Laplacian transform still renders more useful EEG measures than those derived from surface potentials. Undoubtedly, the usefulness needs to be determined with regards to the research objective for each application, which will likely be different for clinical or basic research questions and when focusing on individual or group data.

For group comparisons ($N = 17$), we have shown that a 31-channel EEG montage is entirely appropriate for the analysis of typical auditory ERP components (e.g., N1, N2, P3), revealing effectively the same waveforms and topographies at these sites compared to the original 129-channel ERPs (Kayser and Tenke, 2006b). Moreover, spherical spline interpolations of the data at sites missing in the low-density montage revealed reasonable approximations of the high-density data. The reason for this convergence between low- and high-density CSDs can be attributed to the spatial low-pass filter imposed on the data by averaging ERPs across many individuals, which will remove spatial and temporal noise that is unrelated to the grand mean ERPs.

Other examples of low-density CSD applications involve basic and applied research applications concerned with focal, motor-related activations (e.g., Amengual et al., 2014; Burle et al., 2015; Meckler et al., 2011; Vidal et al., 2003, 2015). Particularly in clinical settings, for which high- resolution EEG is often not feasible, the surface Laplacian transformation can maximize the signal-to-noise ratio for the measure of interest (e.g., Cincotti et al., 2004; McFarland, 2015; McFarland et al., 1997). In the latter case, the merits of surface Laplacian are specifically exploited for individual data.

Another consideration is that low spatial sampling (i.e., less than 30 channels) may provide as accurate or even better surface Laplacian estimates than those obtained from dense electrode arrays (128 or more channels) in the presence of high spatial frequency noise (Babiloni et al., 1995). Under these conditions, low spatial density as well as reduced spline flexibility will effectively counteract EEG recording noise and other variations in signal quality, including topographical distortions caused by electrode placements or electrolyte bridging (e.g., Tenke and Kayser, 2001; Alschuler et al., 2014), and render more reliable CSD estimates (cf. Tenke and Kayser, 2012). While this may come at the costs of being less precise (cf. Fig. 7), these estimates are nevertheless more useful for the overall research purpose.

Accordingly, high-density EEG recordings are neither imperative for the surface Laplacian computation nor will they in and of themselves guarantee better or more reliable CSD estimates.

3.4. Susceptibility to noise

Because the surface Laplacian is inherently computed from signal differences (i.e., second spatial derivative), and differences are typically more variable than the original data, it may be reasoned that one of the costs of the surface Laplacian transform is a greater sensitivity to the level of noise in the data (e.g., Bradshaw and Wikswo, 2001; Murray et al., 2008). Systematic manipulations have shown that the surface Laplacian estimation error increased proportionally with magnitude and spatial frequency of simulated noise levels (Babiloni et al., 1995). The particular concern is that because the surface Laplacian will amplify higher over lower spatial frequencies, signal distortions will be caused by high frequency noise, including recording artifacts (Bradshaw and Wikswo, 2001). While these negative effects can be counteracted by heavier regularization and use of more rigid splines, this comes with a loss in spatial resolution, as one of the declared goals of using a surface Laplacian is to enhance the spatial resolution of the EEG signal. Obviously, this concern constitutes a paradox of sorts with the lamented signal loss of low spatial frequencies discussed above. The worry about the negative impact of noise also appears to be at odds with evidence showing that the surface Laplacian can actually increase the signal-to-noise ratio for specific applications.

As before, from a pragmatic standpoint, the critical question is how differences in noise levels differentially affect SP and SL measures for real EEG data. After reducing the signal-to-noise ratio by limiting the number of trials to compute an error-related negativity, the surface Laplacian was found to render better results than its surface potential counterparts (Cohen, 2014). We manipulated noise levels by evaluating hemifield-dependent N1 asymmetries with nonparametric permutation tests using different sample sizes ($N = 130$, 80, 40, 20, or 10), which did not affect the superior performance of CSD compared to ERP or EEG measures, although overall statistical significance progressively declined with smaller sample size across all data transformations (Kayser and Tenke, 2015).

Thus, while the signal-to-noise ratio should always be a general concern, it seems unfounded to raise this issue as a justification for rejecting surface Laplacian in favor of surface potential measures. To the contrary, the available evidence suggests a better performance of surface Laplacian measures under conditions with reduced signal-to-noise ratio. The only caveat that is required is that the use of surface potentials will not protect against poor data quality.

3.5. Loss of signal at the edge of the EEG montage and other miscellaneous apprehensions

A number of other reservations have repeatedly been cited in addition to the above concerns, including difficulties of computing the surface Laplacian at the edge of the EEG montage, the required explicit knowledge about the recording locations, and the need to quantify the surface Laplacian estimates. While the loss of information at border locations may be a sacrifice for finite difference methods (e.g., Hjorth, 1975), surface Laplacian estimates are readily available for these and at any other location by the use of spherical splines and other continuous interpolations (e.g., Nunez and Srinivasan, 2006; Pascual-Marqui

et al., 1988; Perrin et al., 1989; reviewed by Carvalhaes and de Barros, 2015).

Precise information about where the EEG signals were recorded seems to be an obligatory requirement for any responsible researcher, particularly if these signals are used to infer brain functions. The level of required precision depends on the (implicit) head model, which may be as simple as the 10–20 system and its expansions (e.g., Jurcak et al., 2007; Oostenveld and Praamstra, 2001). Spherical head models appear to be appropriate for many SL applications, particularly for the typical range of spatial frequencies available from a finite number of electrodes (Yao, 2002b).

The surface Laplacian transformation is a spatial transformation that does not alter the data domain, and consequently, CSD values can be treated just like surface potential values (i.e., using the same analytic tools). In fact, the combined used of surface Laplacian with other multivariate approaches, such as PCA (e.g., Kayser and Tenke, 2006a) or ICA (e.g., Fitzgibbon et al., 2015), has demonstrated considerable advantages. However, the challenge of how to identify and quantify appropriate dependent measures for the data at hand cannot be regarded as a valid reservation, because it equally applies to SP and SL data.

4. Concluding remarks

Reference-dependent surface potentials are ambiguous in all key aspects of the EEG signal (polarity, topography, latency). Common approaches to identify and quantify the important characteristics of these data will lead to different results, with the extent of these differences ranging from minor discrepancies to diametrically opposite findings. The surface Laplacian is a unique, linear data transformation that maintains the invariant (i.e., reference-independent) aspects of the EEG signal, thereby resolving all of these ambiguities. As reviewed here, spherical spline interpolation provides a convenient means to obtain continuous estimates of radial current flow at scalp for low- and high-density EEG montages. The CSD distributions represent neuronal generator patterns in space and time that can (and should) be analyzed via the same analytic approaches already employed for surface potentials. Appropriate selection of spline interpolation parameters can counteract known limitations of the surface Laplacian (i.e., spatial high pass) without resorting to the notorious pitfalls of surface potentials. However, more work is still required to study the applicability of SL estimates based on less flexible splines in the context of functional connectivity and coherence for EEG phenomena generated by very large dipole layers, and whether an approach of using SL estimates obtained with different spline flexibility is a sufficient substitute for the strategy of using both the average reference and flexible SL estimates when investigating global functional integration. Other suspected weaknesses, such as higher sensitivity to noise and insensitivity to deep generators, have not been sustained by empirical evidence. For these practical reasons, the continued preferential use of surface potentials for much of EEG and ERP research appears to be counterintuitive and counterproductive.

Supplementary data to this article can be found online at http://dx.doi.org/10.1016/j.ijpsycho.2015.04.012.

Acknowledgments

This work was supported in part by grants MH036295, MH036197, MH082393, MH092250 and MH094356 from the National Institute of Mental Health (NIMH). We greatly appreciate the use of waveform plotting software written and generously provided by Charles L. Brown, III. We are grateful for constructive feedback and helpful comments of Paul L. Nunez and one anonymous reviewer, which resulted in the simulation of expanding dipole layers as a function of spline flexibility.

References

Alschuler, D.M., Tenke, C.E., Bruder, G.E., Kayser, J., 2014. Identifying electrode bridging from electrical distance distributions: a survey of publicly-available EEG data using a new method. Clin. Neurophysiol. 125 (3), 484–490.
Amengual, J.L., Münte, T.F., Marco-Pallares, J., Rojo, N., Grau-Sanchez, J., Rubio, F., Duarte, E., Grau, C., Rodriguez Fornells, A., 2014. Overactivation of the supplementary motor area in chronic stroke patients. J. Neurophysiol. 112 (9), 2251–2263.
Babiloni, F., Babiloni, C., Fattorini, L., Carducci, F., Onorati, P., Urbano, A., 1995. Performances of surface Laplacian estimators: a study of simulated and real scalp potential distributions. Brain Topogr. 8 (1), 35–45.
Babiloni, F., Babiloni, C., Carducci, F., Fattorini, L., Onorati, P., Urbano, A., 1996. Spline Laplacian estimate of EEG potentials over a realistic magnetic resonance-constructed scalp surface model. Electroencephalogr. Clin. Neurophysiol. 98 (4), 363–373.
Babiloni, F., Babiloni, C., Carducci, F., Gaudio, M.D., Onorati, P., Urbano, A., 1997. A high resolution EEG method based on the correction of the surface Laplacian estimate for the subject's variable scalp thickness. Electroencephalogr. Clin. Neurophysiol. 103 (4), 486–492.
Barry, R.J., De Blasio, F.M., 2013. Sequential processing in the equiprobable auditory Go/NoGo task: a temporal PCA study. Int. J. Psychophysiol. 89 (1), 123–127.
Berg, P., 2006. Dipole simulator (Version 3.3.0.4). [http://www.besa.de/updates/tools].
Berger, H., 1929. Über das Elektroenkephalogramm des Menschen. Arch. Psychiatry Nervenkr. 87, 527–570.
Bertrand, O., Perrin, F., Pernier, J., 1985. A theoretical justification of the average reference in topographic evoked potential studies. *Electroenceph*. Clin. Neurophysiol. 62 (6), 462–464.
Bortel, R., Sovka, P., 2007. Regularization techniques in realistic Laplacian computation. IEEE Trans. Biomed. Eng. 54 (11), 1993–1999.
Bortel, R., Sovka, P., 2013. Potential approximation in realistic Laplacian computation. Clin. Neurophysiol. 124 (3), 462–473.
Bradshaw, L.A., Wikswo Jr., J.P., 2001. Spatial filter approach for evaluation of the surface Laplacian of the electroencephalogram and magnetoencephalogram. Ann. Biomed. Eng. 29 (3), 202–213.
Burle, B., Spieser, L., Roger, C., Casini, L., Hasbroucq, T., Vidal, F., 2015. Spatial and temporal resolution of EEG: is it really black and white? A scalp current density view. Int. J. Psychophysiol. 97 (3), 210–220.
Carvalhaes, C.G., de Barros, J.A., 2015. The surface Laplacian technique in EEG: theory and methods. Int. J. Psychophysiol. 97 (3), 174–188.
Carvalhaes, C.G., Suppes, P., 2011. A spline framework for estimating the EEG surface laplacian using the Euclidean metric. Neural Comput. 23 (11), 2974–3000.
Chen, A.C., Feng, W., Zhao, H., Yin, Y., Wang, P., 2008. EEG default mode network in the human brain: spectral regional field powers. Neuroimage 41 (2), 561–574.
Cincotti, F., Babiloni, C., Miniussi, C., Carducci, F., Moretti, D., Salinari, S., Pascual-Marqui, R., Rossini, P.M., Babiloni, F., 2004. EEG deblurring techniques in a clinical context. Methods Inf. Med. 43 (1), 114–117.
Coan, J.A., Allen, J.J., 2004. Frontal EEG asymmetry as a moderator and mediator of emotion. Biol. Psychol. 67 (1–2), 7–50.
Cohen, M.X., 2015. Comparison of different spatial transformations applied to EEG data: A case study of error processing. Int. J. Psychophysiol. 97 (3), 245–257.
Davidson, R.J., 1998. Anterior electrophysiological asymmetries, emotion, and depression: conceptual and methodological conundrums. Psychophysiology 35 (5), 607–614.
Dien, J., 1998. Issues in the application of the average reference: review, critiques, and recommendations. Behav. Res. Methods Instrum. Comput. 30 (1), 34–43.
Donchin, E., 1981. Surprise!…Surprise? Psychophysiology 18 (5), 493–513.
Donchin, E., Coles, M.G.H., 1988. Is the P300 component a manifestation of context updating? Behav. Brain Sci. 11 (3), 357–374.
Fabiani, M., Friedman, D., 1995. Changes in brain activity patterns in aging: the novelty oddball. Psychophysiology 32 (6), 579–594.
Falkenstein, M., Hoormann, J., Christ, S., Hohnsbein, J., 2000. ERP components on reaction errors and their functional significance: a tutorial. Biol. Psychol. 51 (2–3), 87–107.
Fein, G., Raz, J., Brown, F.F., Merrin, E.L., 1988. Common reference coherence data are confounded by power and phase effects. Electroencephalogr. Clin. Neurophysiol. 69 (6), 581–584.
Fitzgibbon, S.P., DeLosAngeles, D., Lewis, T.W., Powers, D.M.W., Whitham, E.M., Willoughby, J.O., Pope, K.J., 2015. Surface Laplacian of scalp electrical signals and independent component analysis resolve EMG contamination of electroencephalogram. Int. J. Psychophysiol. 97 (3), 277–284.
Freeman, J.A., Nicholson, C., 1975. Experimental optimization of current source-density technique for anuran cerebellum. J. Neurophysiol. 38 (2), 369–382.
Galaburda, A.M., 1995. Anatomic basis of cerebral dominance. In: Davidson, R.J., Hugdahl, K. (Eds.), Brain Asymmetry. MIT Press, Cambridge, MA, pp. 51–73.
Gehring, W.J., Goss, B., Coles, M.G.H., Meyer, D.E., Donchin, E., 1993. A neural system for error-detection and compensation. Psychol. Sci. 4 (6), 385–390.
Geschwind, N., Levitsky, W., 1968. Human brain: left-right asymmetries in temporal speech region. Science 161 (837), 186–187.
Gevins, A., 1996. High resolution evoked potentials of cognition. Brain Topogr. 8 (3), 189–199.
Gevins, A., 1998. The future of electroencephalography in assessing neurocognitive functioning. Electroencephalogr. Clin. Neurophysiol. 106 (2), 165–172.
Gevins, A., Cutillo, B., Smith, M.E., 1995. Regional modulation of high resolution evoked potentials during verbal and non-verbal matching tasks. Electroencephalogr. Clin. Neurophysiol. 94 (2), 129–147.
Gevins, A., Le, J., Leong, H., McEvoy, L.K., Smith, M.E., 1999. Deblurring. J. Clin. Neuropsychol. 16 (3), 204–213.

Giard, M.H., Perrin, F., Pernier, J., Bouchet, P., 1990. Brain generators implicated in the processing of auditory stimulus deviance: a topographic event-related potential study. Psychophysiology 27 (6), 627–640.
Giard, M.H., Besle, J., Aguera, P.E., Gomot, M., Bertrand, O., 2014. Scalp current density mapping in the analysis of mismatch negativity paradigms. Brain Topogr. 27 (4), 428–437.
Guevara, R., Velazquez, J.L., Nenadovic, V., Wennberg, R., Senjanovic, G., Dominguez, L.G., 2005. Phase synchronization measurements using electroencephalographic recordings: what can we really say about neuronal synchrony? Neuroinformatics 3 (4), 301–314.
He, B., Lian, J., Li, G., 2001. High-resolution EEG: a new realistic geometry spline Laplacian estimation technique. Clin. Neurophysiol. 112 (5), 845–852.
Hjorth, B., 1975. An on-line transformation of EEG scalp potentials into orthogonal source derivations. *Electroenceph*. Clin. Neurophysiol. Suppl. 39 (5), 526–530.
Hjorth, B., 1980. Source derivation simplifies topographical EEG interpretation. Am. J. EEG Technol. 20, 121–132.
Hoffmann, S., Falkenstein, M., 2012. Predictive information processing in the brain: errors and response monitoring. Int. J. Psychophysiol. 83 (2), 208–212.
Hsieh, L.T., Ranganath, C., 2014. Frontal midline theta oscillations during working memory maintenance and episodic encoding and retrieval. Neuroimage 85, 721–729.
Joyce, C., Rossion, B., 2005. The face-sensitive N170 and VPP components manifest the same brain processes: the effect of reference electrode site. Clin. Neurophysiol. 116 (11), 2613–2631.
Junghöfer, M., Elbert, T., Leiderer, P., Berg, P., Rockstroh, B., 1997. Mapping EEG-potentials on the surface of the brain: a strategy for uncovering cortical sources. Brain Topogr. 9 (3), 203–217.
Jurcak, V., Tsuzuki, D., Dan, I., 2007. 10/20, 10/10, and 10/5 systems revisited: their validity as relative head-surface-based positioning systems. Neuroimage 34 (4), 1600–1611.
Kayser, J., 2009. Current source density (CSD) interpolation using spherical splines - CSD Toolbox (Version 1.1). Division of Cognitive Neuroscience, New York State Psychiatric Institute (http://psychophysiology.cpmc.columbia.edu/Software/CSDtoolbox).
Kayser, J., Tenke, C.E., 2003. Optimizing PCA methodology for ERP component identification and measurement: theoretical rationale and empirical evaluation. Clin. Neurophysiol. 114 (12), 2307–2325.
Kayser, J., Tenke, C.E., 2006a. Principal components analysis of Laplacian waveforms as a generic method for identifying ERP generator patterns: I. Evaluation with auditory oddball tasks. Clin. Neurophysiol. 117 (2), 348–368.
Kayser, J., Tenke, C.E., 2006b. Principal components analysis of Laplacian waveforms as a generic method for identifying ERP generator patterns: II. Adequacy of low-density estimates. Clin. Neurophysiol. 117 (2), 369–380.
Kayser, J., Tenke, C.E., 2010. In search of the Rosetta Stone for scalp EEG: converging on reference-free techniques. Clin. Neurophysiol. 121 (12), 1973–1975.
Kayser, J., Tenke, C.E., 2015. Hemifield-dependent N1 and event-related theta/delta oscillations: an unbiased comparison of surface Laplacian and common EEG reference choices. Int. J. Psychophysiol. 97 (3), 258–270.
Kayser, J., Tenke, C.E., Gates, N.A., Bruder, G.E., 2007. Reference-independent ERP old/new effects of auditory and visual word recognition memory: joint extraction of stimulus- and response-locked neuronal generator patterns. Psychophysiology 44 (6), 949–967.
Kayser, J., Tenke, C.E., Gil, R.B., Bruder, G.E., 2009. Stimulus- and response-locked neuronal generator patterns of auditory and visual word recognition memory in schizophrenia. Int. J. Psychophysiol. 73 (3), 186–206.
Kayser, J., Tenke, C.E., Kroppmann, C.J., Fekri, S., Alschuler, D.M., Gates, N.A., Gil, R., Harkavy Friedman, J.M., Jarskog, L.F., Bruder, G.E., 2010. Current source density (CSD) old/new effects during recognition memory for words and faces in schizophrenia and in healthy adults. Int. J. Psychophysiol. 75 (2), 194–210.
Kayser, J., Tenke, C.E., Kroppmann, C.J., Alschuler, D.M., Fekri, S., Ben-David, S., Corcoran, C.M., Bruder, G.E., 2014. Auditory event-related potentials and alpha oscillations in the psychosis prodrome: neuronal generator patterns during a novelty oddball task. Int. J. Psychophysiol. 91 (2), 104–120.
Klimesch, W., 1999. EEG alpha and theta oscillations reflect cognitive and memory performance: a review and analysis. Brain Res. Brain Res. Rev. 29 (2–3), 169–195.
Law, S.K., Nunez, P.L., Wijesinghe, R.S., 1993a. High-resolution EEG using spline generated surface Laplacians on spherical and ellipsoidal surfaces. IEEE Trans. Biomed. Eng. 40 (2), 145–153.
Law, S.K., Rohrbaugh, J.W., Adams, C.M., Eckardt, M.J., 1993b. Improving spatial and temporal resolution in evoked EEG responses using surface Laplacians. Electroenceph. Clin. Neurophysiol. 88 (4), 309–322.
Lehmann, D., Skrandies, W., 1980. Reference-free identification of components of checkerboard- evoked multichannel potential fields. Electroencephalogr. Clin. Neurophysiol. 48 (6), 609–621.
Marzetti, L., Nolte, G., Perrucci, M.G., Romani, G.L., Del Gratta, C., 2007. The use of standardized infinity reference in EEG coherency studies. Neuroimage 36 (1), 48–63.
May, P.J., Tiitinen, H., 2010. Mismatch negativity (MMN), the deviance-elicited auditory deflection, explained. Psychophysiology 47 (1), 66–122.
McFarland, D.J., 2015. The advantages of the surface Laplacian in brain-computer interface research. Int. J. Psychophysiol. 97 (3), 271–276.
McFarland, D.J., McCane, L.M., David, S.V., Wolpaw, J.R., 1997. Spatial filter selection for EEG-based communication. Electroencephalogr. Clin. Neurophysiol. 103 (3), 386–394.
Meckler, C., Allain, S., Carbonnell, L., Hasbroucq, T., Burle, B., Vidal, F., 2011. Executive control and response expectancy: a Laplacian ERP study. Psychophysiology 48 (3), 303–311.
Michel, C.M., Murray, M.M., Lantz, G., Gonzalez, S., Spinelli, L., Grave de Peralta, R., 2004. EEG source imaging. Clin. Neurophysiol. 115 (10), 2195–2222.
Michie, P.T., 2001. What has MMN revealed about the auditory system in schizophrenia? Int. J. Psychophysiol. 42 (2), 177–194.
Müller-Gass, A., Stelmack, R.M., Campbell, K.B., 2005. "… and were instructed to read a self-selected book while ignoring the auditory stimuli": the effects of task demands on the mismatch negativity. Clin. Neurophysiol. 116 (9), 2142–2152.
Murray, M.M., Brunet, D., Michel, C.M., 2008. Topographic ERP analyses: a step-by-step tutorial review. Brain Topogr. 20 (4), 249–264.
Näätänen, R., 1990. The role of attention in auditory information processing as revealed by event-related potentials and other brain measures of cognitive function. Behav. Brain Sci. 13, 201–288.
Näätänen, R., Picton, T.W., 1987. The N1 wave of the human electric and magnetic response to sound: a review and an analysis of the component structure. Psychophysiology 24 (4), 375–425.
Näätänen, R., Kujala, T., Escera, C., Baldeweg, T., Kreegipuu, K., Carlson, S., Ponton, C., 2012. The mismatch negativity (MMN) – a unique window to disturbed central auditory processing in ageing and different clinical conditions. Clin. Neurophysiol. 123 (3), 424–458.
Nieuwenhuis, S., Aston-Jones, G., Cohen, J.D., 2005. Decision making, the P3, and the locus coeruleus-norepinephrine system. Psychol. Bull. 131 (4), 510–532.
Nunez, P., 1981. Electric fields of the brain. Oxford University Press, New York.
Nunez, P.L., Pilgreen, K.L., 1991. The spline-Laplacian in clinical neurophysiology: a method to improve EEG spatial resolution. J. Clin. Neuropsychol. 8 (4), 397–413.
Nunez, P.L., Srinivasan, R., 2006. Electric fields of the brain: the neurophysics of EEG. Oxford University Press, New York.
Nunez, P.L., Srinivasan, R., 2014. Neocortical dynamics due to axon propagation delays in cortico-cortical fibers: EEG traveling and standing waves with implications for top-down influences on local networks and white matter disease. Brain Res. 1542, 138–166.
Nunez, P.L., Westdorp, A.F., 1994. The surface Laplacian, high resolution EEG and controversies. Brain Topogr. 6 (3), 221–226.
Nunez, P.L., Silberstein, R.B., Cadusch, P.J., Wijesinghe, R.S., Westdorp, A.F., Srinivasan, R., 1994. A theoretical and experimental study of high resolution EEG based on surface Laplacians and cortical imaging. Electroencephalogr. Clin. Neurophysiol. 90 (1), 40–57.
Nunez, P.L., Srinivasan, R., Westdorp, A.F., Wijesinghe, R.S., Tucker, D.M., Silberstein, R.B., Cadusch, P.J., 1997. EEG coherency. I: Statistics, reference electrode, volume conduction, Laplacians, cortical imaging, and interpretation at multiple scales. Electroencephalogr. Clin. Neurophysiol. 103 (5), 499–515.
Nunez, P.L., Silberstein, R.B., Shi, Z., Carpenter, M.R., Srinivasan, R., Tucker, D.M., Doran, S.M., Cadusch, P.J., Wijesinghe, R.S., 1999. EEG coherency II: experimental comparisons of multiple measures. Clin. Neurophysiol. 110 (3), 469–486.
Oostenveld, R., Praamstra, P., 2001. The five percent electrode system for high-resolution EEG and ERP measurements. Clin. Neurophysiol. 112 (4), 713–719.
Osselton, J.W., 1965. Acquisition of EEG data by bipolar, unipolar and average reference methods: a theoretical comparison. Electroencephalogr. Clin. Neurophysiol. 19 (5), 527–528.
Pascual-Marqui, R.D., Gonzalez-Andino, S.L., Valdes-Sosa, P.A., Biscay-Lirio, R., 1988. Current source density estimation and interpolation based on the spherical harmonic Fourier expansion. Int. J. Neurosci. 19 (3–4), 237–249.
Pascual-Marqui, R.D., Michel, C.M., Lehmann, D., 1994. Low resolution electromagnetic tomography: a new method for localizing electrical activity in the brain. Int. J. Psychophysiol. 18 (1), 49–65.
Perrin, F., Bertrand, O., Pernier, J., 1987. Scalp current density mapping: value and estimation from potential data. IEEE Trans. Biomed. Eng. 34 (4), 283–288.
Perrin, F., Pernier, J., Bertrand, O., Echallier, J.F., 1989. Spherical splines for scalp potential and current density mapping [Corrigenda EEG 02274, EEG Clin. Neurophysiol., 1990, 76, 565]. Electroencephalogr. Clin. Neurophysiol. 72 (2), 184–187.
Pizzagalli, D., Pascual Marqui, R.D., Nitschke, J.B., Oakes, T.R., Larson, C.L., Abercrombie, H.C., Schaefer, S.M., Koger, J.V., Benca, R.M., Davidson, R.J., 2001. Anterior cingulate activity as a predictor of degree of treatment response in major depression: evidence from brain electrical tomography analysis. Am. J. Psychiatry 158 (3), 405–415.
Polich, J., 2007. Updating P300: an integrative theory of P3a and P3b. Clin. Neurophysiol. 118 (10), 2128–2148.
Roux, F., Uhlhaas, P.J., 2014. Working memory and neural oscillations: alpha-gamma versus theta-gamma codes for distinct WM information? Trends Cogn. Sci. 18 (1), 16–25.
Sauseng, P., Klimesch, W., Schabus, M., Doppelmayr, M., 2005. Fronto-parietal EEG coherence in theta and upper alpha reflect central executive functions of working memory. Int. J. Psychophysiol. 57 (2), 97–103.
Scheeringa, R., Bastiaansen, M.C., Petersson, K.M., Oostenveld, R., Norris, D.G., Hagoort, P., 2008. Frontal theta EEG activity correlates negatively with the default mode network in resting state. Int. J. Psychophysiol. 67 (3), 242–251.
Scherg, M., von Cramon, D., 1985. Two bilateral sources of the late AEP as identified by a spatio-temporal dipole model. Electroenceph. Clin. Neurophysiol. 62 (1), 32–44.
Schiff, S.J., 2005. Dangerous phase. Neuroinformatics 3 (4), 315–318.
Shibasaki, H., Nakamura, M., Sugi, T., Nishida, S., Nagamine, T., Ikeda, A., 2014. Automatic interpretation and writing report of the adult waking electroencephalogram. Clin. Neurophysiol. 125 (6), 1081–1094.
Spencer, K.M., Dien, J., Donchin, E., 1999. A componential analysis of the ERP elicited by novel events using a dense electrode array. Psychophysiology 36 (3), 409–414.
Spencer, K.M., Dien, J., Donchin, E., 2001. Spatiotemporal analysis of the late ERP responses to deviant stimuli. Psychophysiology 38 (2), 343–358.
Srinivasan, R., 1999. Spatial structure of the human alpha rhythm: global correlation in adults and local correlation in children. Clin. Neurophysiol. 110 (8), 1351–1362.
Srinivasan, R., Nunez, P.L., Tucker, D.M., Silberstein, R.B., Cadusch, P.J., 1996. Spatial sampling and filtering of EEG with spline laplacians to estimate cortical potentials. Brain Topogr. 8 (4), 355–366.

Srinivasan, R., Nunez, P.L., Silberstein, R.B., 1998a. Spatial filtering and neocortical dynamics: estimates of EEG coherence. IEEE Trans. Biomed. Eng. 45 (7), 814–826.
Srinivasan, R., Tucker, D.M., Murias, M., 1998b. Estimating the spatial Nyquist of the human EEG. Behav. Res. Methods Instrum. Comput. 30 (1), 8–19.
Stam, C.J., van Straaten, E.C., 2012. The organization of physiological brain networks. Clin. Neurophysiol. 123 (6), 1067–1087.
Stone, M., 1974. Cross-validatory choice and assessment of statistical predictions. J. R. Stat. Soc. B 36 (2), 111–147.
Sutton, S., Ruchkin, D.S., 1984. The late positive complex: advances and new problems. In: Karrer, R., Cohen, J., Tueting, P. (Eds.), Annals of the New York Academy of Sciences. Brain and information: Event-related potentials vol. 425. New York Academy of Sciences, New York, pp. 1–23.
Sutton, S., Braren, M., Zubin, J., John, E.R., 1965. Evoked potential correlates of stimulus uncertainty. Science 150, 1187–1188.
Tenke, C.E., Kayser, J., 2001. A convenient method for detecting electrolyte bridges in multichannel electroencephalogram and event-related potential recordings. Clin. Neurophysiol. 112 (3), 545–550.
Tenke, C.E., Kayser, J., 2005. Reference-free quantification of EEG spectra: combining current source density (CSD) and frequency principal components analysis (fPCA). Clin. Neurophysiol. 116 (12), 2826–2846.
Tenke, C.E., Kayser, J., 2012. Generator localization by current source density (CSD): implications of volume conduction and field closure at intracranial and scalp resolutions. Clin. Neurophysiol. 123 (12), 2328–2345.
Tenke, C.E., Kayser, J., 2015a. Surface Laplacians and phase properties of EEG rhythms: simulated generators in a volume-conduction model. Int. J. Psychophysiol. 97 (3), 285–298.
Tenke, C.E., Kayser, J., 2015b. Posterior EEG alpha at rest and during task performance: comparison of current source density and field potential measures. Int. J. Psychophysiol. 97 (3), 299–309.
Tenke, C.E., Schroeder, C.E., Arezzo, J.C., Vaughan Jr., H.G., 1993. Interpretation of high-resolution current source density profiles: a simulation of sublaminar contributions to the visual evoked potential. Exp. Brain Res. 94 (2), 183–192.
Tenke, C.E., Kayser, J., Fong, R., Leite, P., Towey, J.P., Bruder, G.E., 1998. Response- and stimulus-related ERP asymmetries in a tonal oddball task: a Laplacian analysis. Brain Topogr. 10 (3), 201–210.
Tenke, C.E., Kayser, J., Shankman, S.A., Griggs, C.B., Leite, P., Stewart, J.W., Bruder, G.E., 2008. Hemispatial PCA dissociates temporal from parietal ERP generator patterns: CSD components in healthy adults and depressed patients during a dichotic oddball task. Int. J. Psychophysiol. 67 (1), 1–16.
Tenke, C.E., Kayser, J., Stewart, J.W., Bruder, G.E., 2010. Novelty P3 reductions in depression: characterization using principal components analysis (PCA) of current source density (CSD) waveforms. Psychophysiology 47 (1), 133–146.
Tenke, C.E., Kayser, J., Manna, C.G., Fekri, S., Kroppmann, C.J., Schaller, J.D., Alschuler, D.M., Stewart, J.W., McGrath, P.J., Bruder, G.E., 2011. Current source density measures of electroencephalographic alpha predict antidepressant treatment response. Biol. Psychiatry 70 (4), 388–394.
Tucker, D.M., 1993. Spatial sampling of head electrical fields: the geodesic sensor net. *Electroenceph.* Clin. Neurophysiol. 87 (3), 154–163.
van Boxtel, G.J.M., 1998. Computational and statistical methods for analyzing event-related potential data. Behav. Res. Methods Instrum. Comput. 30 (1), 87–102.
van Noordt, S.J., Segalowitz, S.J., 2012. Performance monitoring and the medial prefrontal cortex: a review of individual differences and context effects as a window on self-regulation. Front. Hum. Neurosci. 6 (197), 1–16.
van Veen, V., Carter, C.S., 2002. The anterior cingulate as a conflict monitor: fMRI and ERP studies. Physiol. Behav. 77 (4–5), 477–482.
Verleger, R., 1997. On the utility of P3 latency as an index of mental chronometry. Psychophysiology 34 (2), 131–156.
Vidal, F., Hasbroucq, T., Grapperon, J., Bonnet, M., 2000. Is the 'error negativity' specific to errors? Biol. Psychol. 51 (2–3), 109–128.
Vidal, F., Grapperon, J., Bonnet, M., Hasbroucq, T., 2003. The nature of unilateral motor commands in between-hand choice tasks as revealed by surface Laplacian estimation. Psychophysiology 40 (5), 796–805.
Vidal, F., Burle, B., Spieser, L., Carbonnell, L., Meckler, C., Casini, L., Hasbroucq, T., 2015. Linking EEG signals, brain functions and mental operations: advantages of the Laplacian transformation. Int. J. Psychophysiol. 97 (3), 221–232.
Wang, K., Begleiter, H., 1999. Local polynomial estimate of surface Laplacian. Brain Topogr. 12 (1), 19–29.
Witelson, S.F., Kigar, D.L., 1988. Asymmetry in brain function follows asymmetry in anatomical form: gross, microscopic, postmortem and imaging studies. In: Boller, F., Grafman, J. (Eds.), Handbook of Neuropsychology vol. 1. Amsterdam, Elsevier, pp. 111–142.
Yao, D., 2000. High-resolution EEG mappings: a spherical harmonic spectra theory and simulation results. Clin. Neurophysiol. 111 (1), 81–92.
Yao, D., 2002a. High-resolution EEG mapping: a radial-basis function based approach to the scalp Laplacian estimate. Clin. Neurophysiol. 113 (6), 956–967.
Yao, D., 2002b. The theoretical relation of scalp Laplacian and scalp current density of a spherical shell head model. Phys. Med. Biol. 47 (12), 2179–2185.